博士論文

Interaction of cesium with calcium silicate insulator materials

(セシウムとカルシウムシリケート保温材との相互作用に関する研究)

リザール ムハンマド

Table of contents

List of figures

List of tables

Abstract

In this doctoral thesis, the series of experimental studies consisting of batch-type adsorption, thermochemical analysis, and gas-solid interaction was conducted to investigate (chemical) interaction between calcium silicate insulator material and cesium. The bulk use of calcium silicate insulation in the nuclear power station is of concern when a severe accident occurs the interaction will be highly encountered. Author firstly investigated the room-temperature batch adsorption of cesium solution onto calcium silicate to obtain kinetics and concentration-dependency adsorption behavior at such conditions. It was found through adsorption kinetics analysis that the adsorption process of cesium followed the pseudo-second order reaction model that highly indicated chemisorption of cesium. Since the interaction of calcium silicate and cesium would also involve high temperature condition, the analyses to determine such temperature of reaction occurrence under Ar-5%H_2 and Ar-4%H_2-20%H_2O atmosphere were carried out using thermogravimetry-differential thermal analysis (TG-DTA). The simulant fission product in this part of study was cesium hydroxide (CsOH). The results showed, regardless of the atmosphere types, that chemical interaction occurred between calcium silicate insulator material and

cesium hydroxide in temperature of 575-730°C with the formation of cesium aluminum silicate ($CsAlSiO_4$). Due to the likely formation involved aluminum which was the impurity in calcium silicate insulation, the benchmark tests using reagent-grade $CaSiO_3$ were performed to unveil it. The results confirmed that without such an element in the samples, no cesium compound was formed as previously obtained in TG-DTA experiments. The last part of the study was performed to comprehend gas-solid interaction of steam containing cesium with calcium silicate using a horizontal electric furnace. Cesium hydroxide was vaporized in the upstream of the furnace and then transported by steam flow to the downstream where calcium silicates were located. To elucidate the prevalence of interaction, two additional calcium silicates from different manufacturers were included in the test. The test was performed under Ar-4%H_2-20%H_2O atmosphere with temperature of 800°C. The XRD patterns of those calsils were changed from their original crystal phase of xonotlite ($Ca_6Si_6O_{17}(OH)_2$) to $CsAlSiO_4$ and Ca_2SiO_4 meaning that the interaction with gaseous cesium hydroxide prevailed. Furthermore, those end-products of calsils, prior to each characterization, were water-dissolved yet the Cs compound ($CsAlSiO_4$) still remained thus implying its insolubility in calsils when interaction once took place.

Chapter 1 Introduction

1.1 Background of research

Following the aftermath of 2011 severe accident at Fukushima Daiichi nuclear power station, internal investigations in the primary containment vessel (PCV) of the units 1 to 3 were intensively performed by Tokyo Electric Power Company Holdings, Inc. (TEPCO) and also as the act of preparatory stage for decommissioning processes [1,2]. The main task of the investigation was to inspect the conditions of the platform inside the PCV, the fallen fuel debris to the control rod drive (CRD), and the pedestal internal structure [2]. The recording devices managed to record the information of temperature, dose rate, and conditions of structures in the vicinity of the pedestal. Particular attention arose to the dose rate distribution of the pedestal area and its vicinity in unit 2. The pedestal area, considering the accident progression, should yield a higher dose rate than those of any other locations in its vicinity, as the area was most affected by molten fuels [3]. In contrast, the measured dose rate was 10 Gy/h at the pedestal area, where most debris should have existed, while 70-80 Gy/h at the vicinity [2]. At the same location, deposits in the form of black pastes and thin pieces of gravel-sized materials were found, which might be one of the causes for the high dose

rate conditions of the surrounding area. Based on the 2017 report by TEPCO [2], Author tries to consolidate information on the condition of dose rates and deposits in the pedestal area of unit 2 into an illustration in Fig. 1.

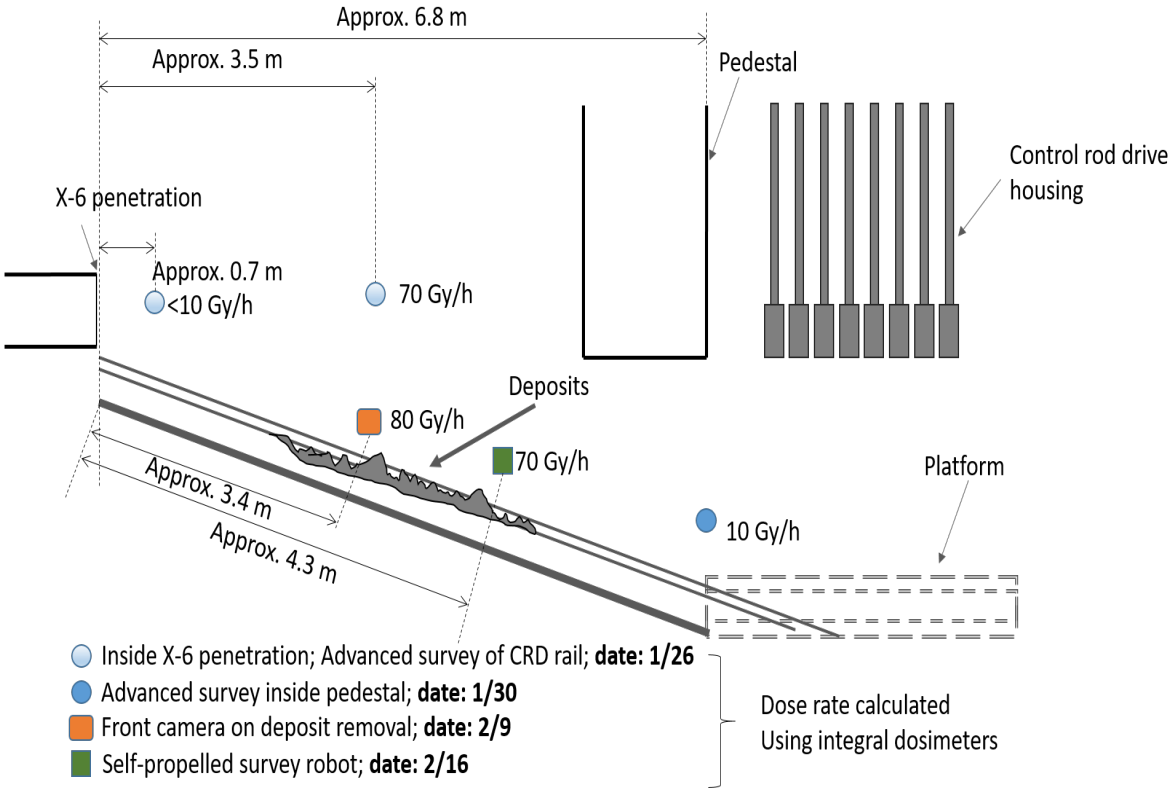

Fig. 1.1 High dose rate condition at the pedestal vicinity of Fukushima Daiichi nuclear power station unit 2.

To date, it has not been resolved how these deposits could be formed and why a high dose rate was produced. Referring to information about the condition and location where these deposits existed, source materials for the deposits must be those used in a large quantity and most affected by high-temperature steam

blast in the PCV, and one of the candidates is a thermal insulation material of the primary piping systems. The hypothesis is originated from two major facts. First, in the same report [2], the pressure history condition of reactor pressure vessels (RPV) was highly fluctuated on March 14 due to pressure balance by safety relief valves (SRVs) and followed by steep pressure drop due to SRV manually set into the fully-open state. The former and more specifically the latter condition could propagate significance influences on the integrity of components of safety relief valves (SRVs) which might be caused by steam flow inside it. Vu et al [4] performed a three-dimensional numerical study on the safety relief valve with oxygen gas as the working fluid to comprehend the appearance of erosion zones. They reported that the flow created multiple vortices, which induced chaotic oscillatory behavior. Second, the location of SRVs and piping systems in unit 2 existed just above the location of deposits, and the appearance characteristics of those deposits were closely related to the insulator materials installed on piping systems. The formation of these deposits is likely originated by high-temperature steam containing fission products such as cesium, leaking from safety relief valves components. Further presumed that the leaked steam directly hit the adjacent line of main steam piping thermal insulation. Then, the interaction of cesium with the material occurs subsequently. However, it should

also be emphasized that the leakage propagation (caused by steam only) and the timing when steam containing cesium (core degradation had progressed) reached leakage point might or might not be in the same time frame.

Recent works focusing on cesium-rich microparticles at the sites near Fukushima Daiichi nuclear power station have indicated, in the samples collected within 60 km, that the provenance of those particles was the end-product interaction of thermal insulation with cesium to which emitted from the reactor unit 1-3 [5–7]. The inference came from the morphological and elemental characteristics possessed by those obtained samples were similar to those of thermal insulation material. Nevertheless, none of published works are available to validate chemical interaction of calcium silicate with cesium and how cesium is retained in the materials particularly at high-temperature condition because most researches are centered on interaction of cesium with other structural materials such as stainless steel [8–12], Inconel [9,13], and concrete [14,15].

1.2 Objectives and scope of the thesis

This subchapter presents briefly the statement of problems, followed by objectives as well as the scope of the doctoral thesis.

1.2.1 Statement of problems

Cesium is placed into the focus of the interacting fission product among other volatile ones because the time between accident and dose rate measurement by TEPCO is approximately six years in which only cesium (i.e., Cs-137: 30 years of half-life) will induce a greater effect on dose rate by gamma radiation. However, the transported cesium from the reactor core could be in some predominant forms such as CsOH, CsI, or Cs_2MoO_4 [16] which may act differently to the insulation material and yielding to a complex interaction. On the other side, the type of thermal insulation material utilized in unit 2 has to be understood regarding its chemical compounds. It is stated in a report of the Japan Nuclear and Industrial Safety Agency (NISA) that the type of thermal insulation in unit 2 is calcium silicate [17].

To date, the interaction between calcium silicate insulator material and cesium, as depicted in the previous subchapter, has not been placed into consideration in fission product transport research at the high-temperature condition. As the consequence, the following major problems can't be resolved: (1) the mechanism of interaction, (2) the temperature when interaction occurs, and (3) the generated products after the interaction. Hence, a structured research study is required to comprehend them.

1.2.2 Objectives

The final objective of this thesis is to provide fundamental knowledge of the interaction of cesium on calcium silicate insulator material. In achieving this objective, some interim objectives are formulated which cover experimentation from room-temperature to high-temperature conditions. Details of each part will be given in subchapter 1.3.

1.2.3. Scope

The thesis is scoped in the interaction of non-radioactive cesium hydroxide (CsOH) and cesium chloride (CsCl; only in the room-temperature study), as the simulant fission products, with calcium silicate insulator material. Upon completing this thesis, it is expected that all the relevant findings could provide robust and significant data for such an interaction in the nuclear primary containment vessel.

1.3 Structure of the thesis

This doctoral thesis is organized into five chapters. The present chapter describes the introductory part of the doctoral thesis which consisting of background, objectives, scope, and structure of the thesis.

Chapter 2 provides the investigation on the interaction of calcium silicate insulator material with cesium in batch-type adsorption experiments. The chapter begins by detailing the specific objective and followed by the introduction of chemical characteristics of calcium silicate insulator material. The procedure taken in performing the experiments, characterization, and post-adsorption analyses proceed the first part of the chapter.

Chapter 3 presents an approach that aims at obtaining reaction temperature and products after interaction between cesium hydroxide and calcium silicate insulator material under reducing and oxidizing atmosphere conditions. The chapter includes pre-experimental procedures and post-experimental analysis involving chemical phase identification, morphological and elemental characterization, and thermodynamics calculation to unveil the chemical compounds of end-products. The benchmark tests using pure chemical reagents are supplemented to the chapter to signify the effect of impurity in calcium silicate when interacting with cesium hydroxide.

Chapter 4 brings the thesis into its last part where describes the investigation in a way of emulating the interaction between steam-cesium hydroxide and calcium silicate block insulation at the obtained temperature from Chapter 3. The chapter begins with the description of high-temperature test

facility and the procedure in performing the experiments and then followed by post-experimental analyses. The calcium silicate blocks from other manufacturers of which differ in impurities' weight percentage are included in the heating test to be analyzed whether the interaction with cesium hydroxide only valid on certain calcium silicate.

Chapter 5 consolidates the major findings of the thesis into the conclusions and then the recommendations for future work are provided.

Two parts of appendices are included in the thesis which consisting of experimental apparatuses used in related chapters and additional results of the thesis that not presented in the main chapters.

Chapter 2 Room-temperature cesium adsorption on calcium silicate thermal insulation material

2.1. Objectives of this chapter

The purposes of the chapter are to elucidate information on time-dependent adsorption of cesium on calcium silicate at room temperature condition and to comprehend the mechanism of adsorption process by time- and concentration-dependency.

One may raise a question, what is the real connection between this part of the thesis and the final target which mainly will be concentrated on high-temperature conditions. The answer can be directed in two circumstances: first, the images and videos footage in TEPCO report [2] have clearly shown the deposits and its surrounding were affected by drops of condensed steam (i.e., mixed with fission products in the atmosphere) from upper region of primary containment vessel and the recorded temperature was 16.5°C while PCV reference temperature was 18.6°C [18] implying that the cesium in condensed form together with water interacted with the calcium silicate at this location within such temperature; second, the adsorption of xonotlite-type calcium silicate (i.e., later

on this chapter, it will be specifically elaborated about this type of material) onto cesium at room-temperature condition, to Author's knowledge, has not been investigated and reported in scientific journal or publication. The sorption of radionuclides to other forms or type of calcium silicate material have been investigated in some studies for immobilization strategies [19–23]. By far, a material used in the only one study by Hassan et al [24] had close similarity to calcium silicate insulation. In their study, the sorption behavior of cesium and europium onto nano-sized calcium silicate (i.e. wollastonite) was investigated. Nevertheless, it is still inapplicable to extend their study to the Fukushima Daiichi case since the insulator material likely consists of different mineral phases of calcium silicate, xonotlite and tobermorite. Therefore, the abovementioned two circumstances are the basis for the room-temperature adsorption study to be conducted to construct fundamental information on the interaction of a calcium silicate insulator material and cesium.

2.2 Calcium silicate insulator material

Calcium silicate insulation material is a common insulator material used in piping systems for high-temperature purposes [25,26]. The material is formed by the hydrothermal reaction between SiO_2 (e.g., source of starting material could be from quartz flour, silica fumes, bentonite, etc.) and $Ca(OH)_2$ in a slurry [25].

Upon the hydrothermal process which undergoes temperature increment, the material turns to tobermorite crystals ($Ca_5Si_6O_{16}(OH)_2 \cdot 4H_2O$) at 180°C [25,27] and proceeds to the formation of xonotlite ($Ca_6Si_6O_{17}(OH)_2$) at about 215°C [25]. Xonotlite and tobermorite crystals belong to the calcium silicate hydrate (C-S-H) system and are structurally similar but the former has double silicate chains parallel to the *b*-axis from layers in the *ab* plane [28]. Hence, it is required to determine the crystal phase of the calcium silicate insulator material used in this study before advancing in the experiments.

2.3. Materials and methods

2.3.1 Materials

For all experiments, Milli-Q grade pure water and analytical-grade chemicals from Wako Pure Chemical Industries were used, unless otherwise noted. Cesium chloride (CsCl) was used in this study. Calcium silicate insulation block, with a specified insulation grade of the nuclear primary coolant system, was used as an adsorbent. Before the experiments, calcium silicate insulation block was cut into small pieces and then ground by an agate mortar.

2.3.2 Characterization

The particle size of the ground calcium silicate insulator material was measured using a laser diffraction size analyzer (SALD-2300, Shimadzu). Field emission scanning electron microscopy equipped with energy dispersive X-ray spectrometry (SEM/EDS, JSM-7610F, JEOL) was used to characterize the morphology and elemental distributions of the samples. A double-sided carbon tape was placed on a sample holder to place the samples and without any further coating. The secondary electron images were obtained at an applied voltage of 15 kV. The powder X-ray diffraction (PXRD) analyses were performed using Rigaku MiniFlex 600, (600 W; Cu Kα radiation) which the scan range was 2θ = 10–80° under continuous mode in a scan speed of 1°/min and step of 0.01°. The applied current and voltage were 15 mA and 40 kV, respectively. The functional group of the material was analyzed with Fourier transform infrared spectrometry (FTIR, Shimadzu FTIR-8400) by the KBr pellet method.

2.3.3 Adsorption Studies

The cesium stock solution was prepared by dissolving CsCl with deionized water. Interaction between calcium silicate insulator material and cesium was realized through batch-type adsorption experiments. The experiments were performed at 25°C using 50 mL conical polypropylene tubes placed inside a

thermostat mechanical shaker. The particle size of ground calcium silicate was measured using a laser diffraction size analyzer (SALD-2300, Shimadzu) as 15.5 ± 0.1 μm (Fig. B.1). For the purpose of adsorption kinetics, 0.02 g and 0.10 g of ground calcium silicate were mixed with 20 mL cesium chloride solution with different initial concentrations of 1.01×10^{-5} and 1.01×10^{-4} M with contact time varied from 0.5 to 98 hours. The pH values of solutions were adjusted between 9.91 and 10.06 by adding 0.1 M HCl or NaOH. Two adsorption isotherms were determined with and without the addition of NaCl as a background electrolyte. For the former, ionic strength was kept constant to 10 mM by proper addition of 1 M NaCl stock solution. In the adsorption isotherm measurements, 0.02 g of ground calcium silicate was mixed with 20 mL cesium solution with the cesium initial concentration varied from 1.3×10^{-6}–3.5×10^{-3} M. Both ionic strength and pH values were set as that of in adsorption kinetics. After the reaction/contact time, the supernatant of solution was filtered using a membrane filter with pore size of 0.45 μm. The filtrate was further diluted with deionized water and 10% nitric acid solution. The final concentrations were measured using inductively coupled plasma mass spectrometry (ICP-MS 7500CS, Agilent). All these experiments were conducted in triplicate.

The adsorption capacity, q_e (mol g^{-1}), and removal percentage, R (%), were determined using equations:

$$q_e = (C_0 - C_e)\frac{V}{m} \quad (2.1)$$

$$R(\%) = \frac{100(C_0 - C_e)}{C_0} \quad (2.2)$$

where q_e is the adsorption capacity at equilibrium time in mol/g, C_0 is the initial concentration in mol/L, C_e is the equilibrium concentration in mol/L, V is the volume of solution in liters, m is the mass of the sorbent in grams.

2.3.4 FTIR sample preparation

At first, all of the calcium silicate solid phases of the three isotherm samples were separated from the corresponding aqueous phases by filtration with a membrane filter of 0.45 μm in the pore size. The obtained solid samples were then dissolved with deionized water, and further separated from the aqueous phase by centrifugation for about 10 minutes with 8000 rpm. After the centrifuge, the process was repeated from separating supernatant until it underwent centrifugation again. When completing the repetition, the separated samples were placed in the heating chamber with temperature of 90°C for 6 hours. The dried samples were then mixed with KBr using agate mortar, in which the weight ratio

of samples/KBr was approximately 1/100. The finely ground materials were formed into pellets to be analyzed in the FTIR spectrometer.

2.4 Calcium silicate insulation material before the adsorption study

The phase identification of calcium silicate with the ICDD (International Center for Diffraction Data) card No. 00-023-0125 for xonotlite ($Ca_6Si_6O_{17}(OH)_2$) and card No. 00-019-1364 for tobermorite ($Ca_5Si_6O_{16}(OH)_2 \bullet 4H_2O$) was determined by X-ray diffraction (XRD). The result shows that the ground calcium silicate insulator material is composed of predominantly xonotlite, Fig. 2.1, which is in agreement with the previous study by Zheng and Wang [25]. Additionally, the micrograph on Fig 3 unveiled the existence of fibers and particle agglomerates, which had Ca/Si atomic ratio of approximately 1.00. This ratio is important supporting evidence to validate the chemical phase of xonotlite identified by XRD since theoretically its starting material of CaO/SiO ratio in C–S–H system should be unity [29].

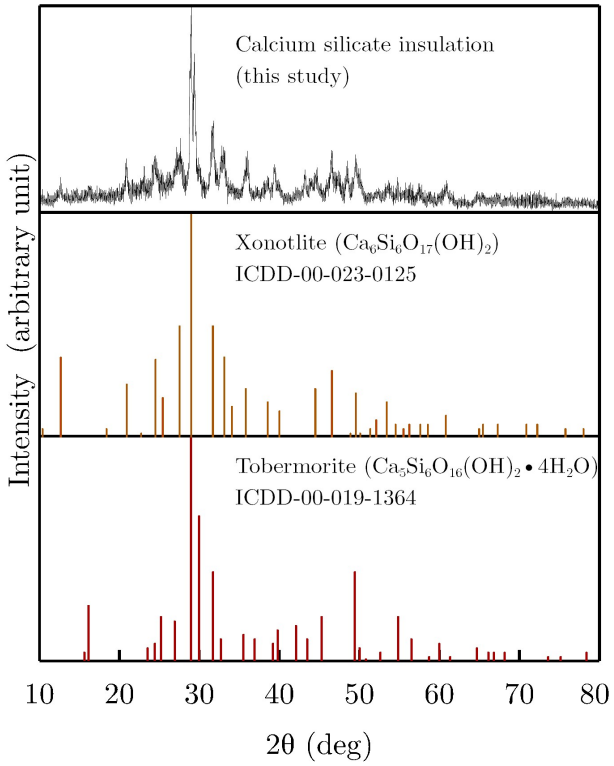

Fig. 2.1 XRD pattern of calcium silicate insulation.

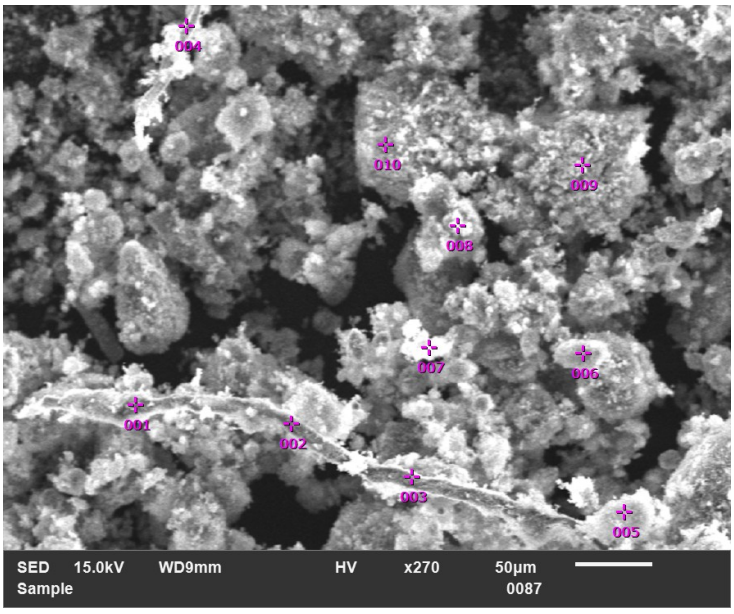

Fig. 2.2 Secondary electron image with elemental point analysis for the calcium silicate material.

Table 2.1 Ca/Si atomic ratio in calcium silicate insulation.

Point location [-]	Ca/Si atomic ratio [-]
001	1.04
002	1.05
003	1.00
004	0.96
005	1.01
006	1.25
007	1.13
008	1.10
009	1.25
010	0.99

2.5 Adsorption kinetics

The adsorption kinetics of cesium on the calcium silicate insulation was evaluated. As shown in Fig. 2.3, the adsorption of cesium reaches equilibrium within 24 hours for those samples with calcium silicate concentration of 1 g/L and 98 hours for that of 5 g/L. Therefore, in the following equilibrium experiments (section 2.6), a contact time of 98 hours was selected.

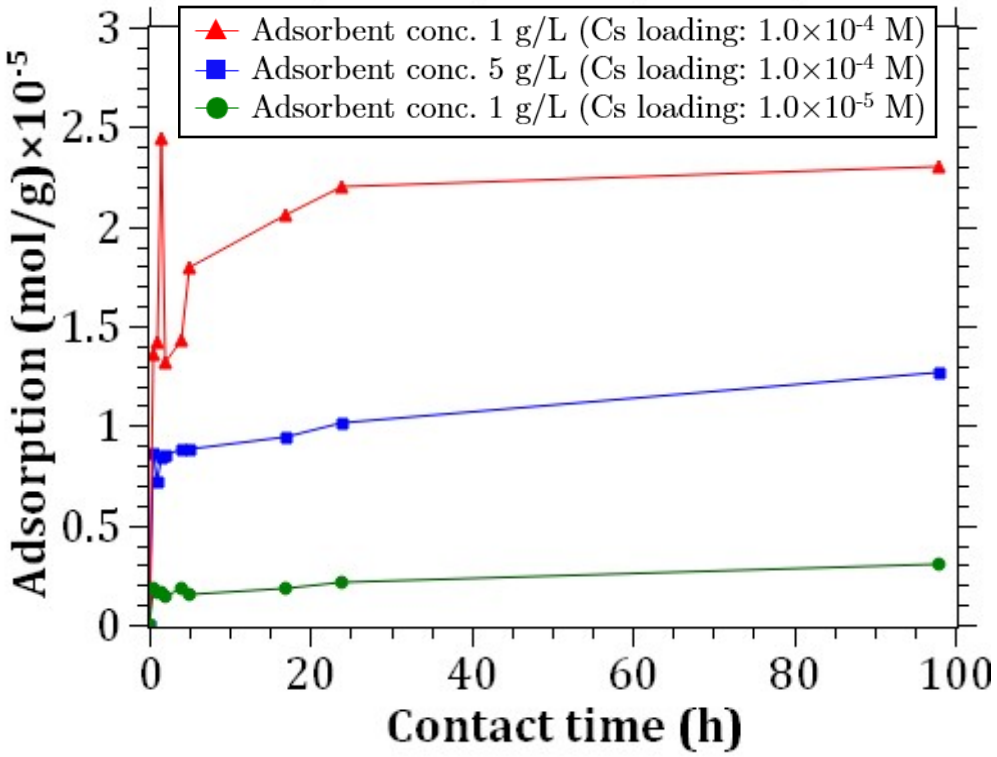

Fig. 2.3 The effect of contact time on cesium adsorption of calcium silicate (Initial concentrations of Cs: 1.0×10^{-5} and 1.0×10^{-4} mol/L; adsorbent concentration: 1 g/L and 5 g/L, temperature: 25°C, maximum contact time: 98 hours).

Adsorption mechanism of cesium on calcium silicate was investigated based on kinetics adsorption models: pseudo-first order and pseudo-second order models. The pseudo-first order rate equation and its linearized form are given in Eqs. (2.3) and (2.4), respectively.

$$\frac{dq_t}{dt} = K_1\left(q_e - q_t\right) \tag{2.3}$$

$$\ln\left(q_e - q_t\right) = \ln q_e - K_1 t \tag{2.4}$$

Where q_t and q_e are the adsorbed amount of Cs^+ (mol/g) at time t (hours) and at equilibrium, respectively; K_1 is pseudo-first order rate constant ($hour^{-1}$). The equilibrium adsorption q_e and rate constants K_1 are calculated by the plot of $\ln(q_e - q_t)$ *vs.* t using Eq. (2.4). On the other hand, the pseudo-second order kinetics model assumes that the reaction kinetics is influenced not merely by cesium concentration (i.e., as in the pseudo-first order model), but also by the active sites on adsorbent. The model and its linearized form are given in Eqs. (2.5) and (2.6) as the following:

$$\frac{dq_t}{dt} = K_2\left(q_e - q_t\right)^2 \tag{2.5}$$

$$\frac{t}{q_t} = \frac{1}{K_2 q_e^2} + \frac{t}{q_e} \tag{2.6}$$

K_2 is pseudo-second order rate constant (g/mol·hour). The equilibrium adsorption q_e and rate constants K_2 are determined by plotting t/q_t *vs.* t using Eq. (6). Two criteria are considered as the basis to determine the most likely adsorption mechanism: (1) relative difference between the adsorbed amount of Cs^+ at equilibrium obtained by the experiment and the kinetics model ($q_{e,experiment}$ and $q_{e,model}$); (2) the correlation coefficients of the fitting (R^2). The favorable condition

is least difference between $q_{e,experiment}$ and $q_{e,model}$, and R^2 close to unity. The obtained parameters of the pseudo-first order and pseudo-second order models are listed on Table 2.2. Based on our experimental data, the adsorption of cesium on calcium silicate was better fitted to the pseudo-second order models, which indicated that Cs^+ was chemisorbed and the adsorption rate of calcium silicate insulator material depended on the active sites rather than Cs^+ concentration in the solution [30]. The subsequent isotherm adsorption and also FTIR analysis in section 2.7 were intended as the supporting proof of such adsorption process.

Table 2.2 Pseudo-first order and pseudo-second order parameters for cesium adsorption on calcium silicate.

Sample	Pseudo-first order kinetics model					Pseudo-second order kinetics model				
	K_1 (h^{-1}) $\times10^{-2}$	$q_{e\ experiment}$ (mol/g) $\times10^{-5}$	$q_{e\ model}$ (mol/g) $\times10^{-5}$	Rel. diff. (%)	R^2	K_2 (g/mol·h) $\times10^{4}$	$q_{e\ experiment}$ (mol/g) $\times10^{-5}$	$q_{e\ model}$ (mol/g) $\times10^{-5}$	Rel. diff. (%)	R^2
0.02 g; 1.0×10^{-4} mol/L	9.42	2.30	1.04	54.6	0.966	3.53	2.30	2.33	0.990	0.999
0.1 g; 1.0×10^{-4} mol/L	2.32	1.27	0.460	64.2	0.808	3.58	1.27	1.28	0.640	0.995
0.02 g; 1.0×10^{-5} mol/L	1.66	0.300	0.140	52.2	0.626	8.18	0.300	0.310	1.25	0.983

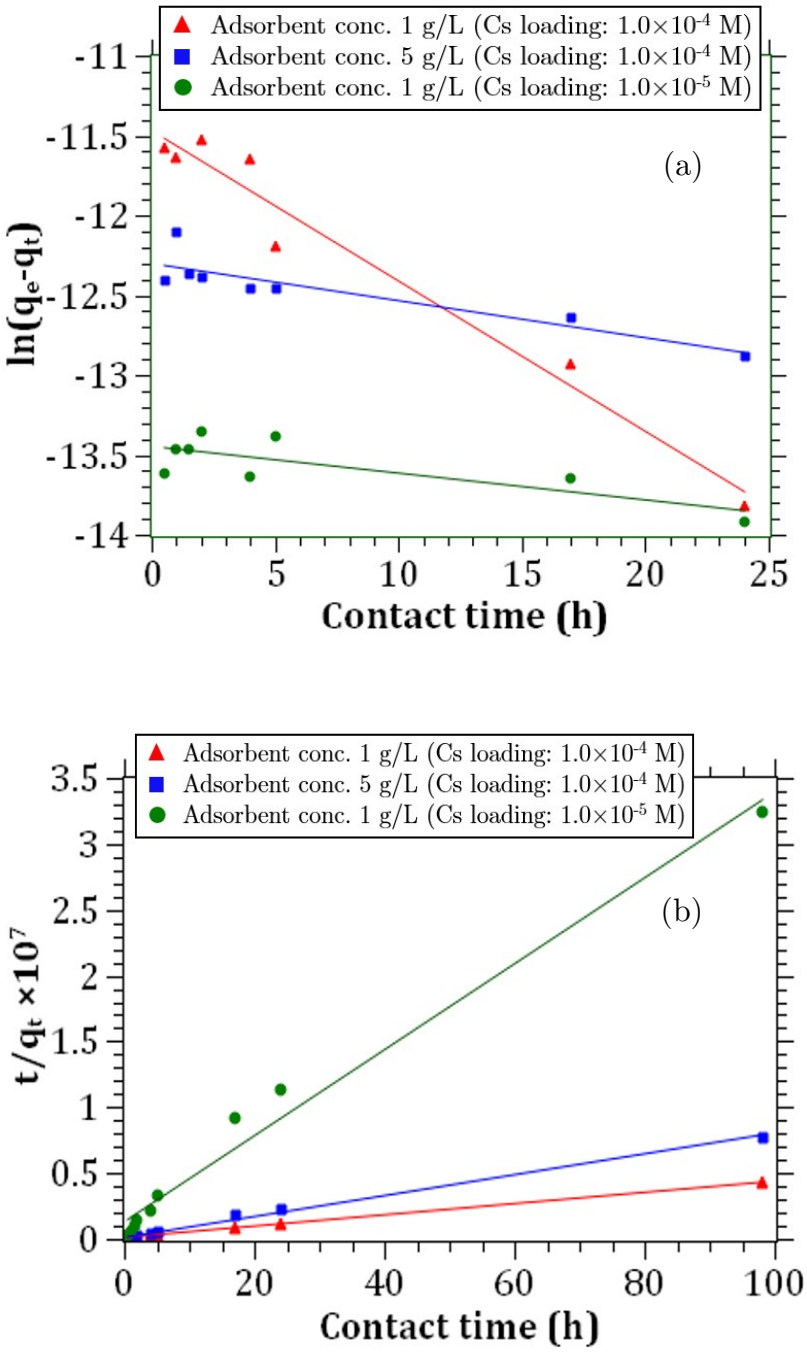

Fig. 2.4 (a) Pseudo-first order kinetics model; (d) Pseudo-second order kinetics model for cesium adsorption on calcium silicate.

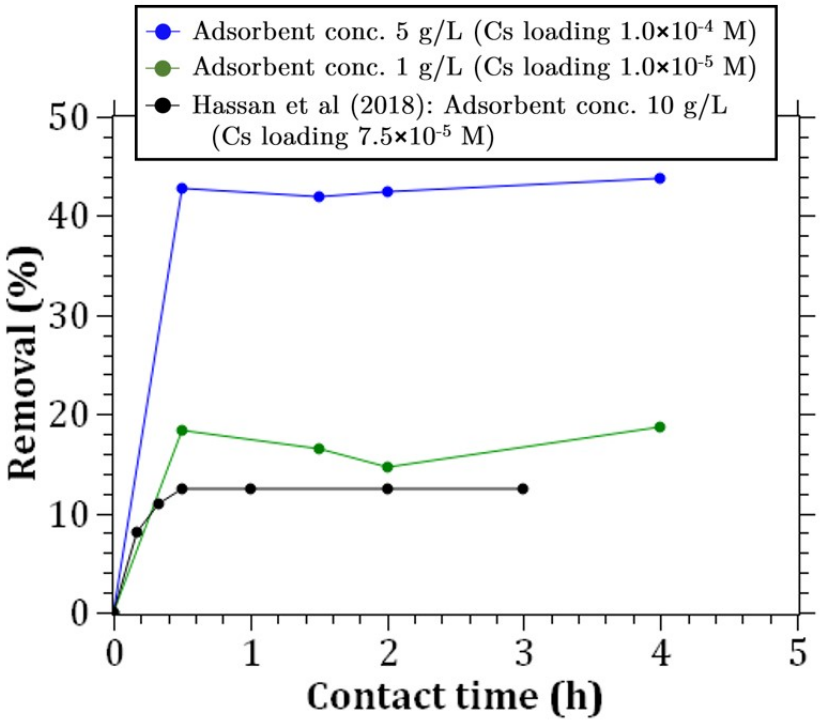

Fig. 2.5 Comparison on cesium removal from aqueous solution by xonotlite-type calcium silicate in this study and wollastonite-type calcium silicate in Hassan et al [24].

The cesium removal percentage by calcium silicate with a different crystal phase, wollastonite, shows a significant difference to our study. This type of calcium silicate has a lower removal percentage even comparing with 1 g/L of xonotlite-type calcium silicate (10 times less adsorbent concentration). Moreover, in term of equilibrium, it had been achieved within 0.5 to 1 hours of contact time while our kinetics study showed equilibrium was achieved within 24 hours (i.e.

those of 1 g/L adsorbent concentrations). These conditions explicitly infer the inapplicability of extending cesium adsorption behavior on wollastonite-type calcium silicate to approach such a phenomenon in calcium silicate insulation of the Fukushima Daiichi NPS case.

2.6 Adsorption isotherm

The adsorption isotherm of cesium to the calcium silicate was investigated to evaluate the performance—as well as to validate findings in adsorption kinetics—with regard to the maximum adsorption capacity (q_m). Its corresponding value represents the theoretical maximum capacity or adsorbent material's ability to adsorb cesium at saturation conditions. The models that had been implemented in our adsorption isotherm experimental data including the two-parameter model: Langmuir [31,32], and the three-parameter model: modified-Brunauer-Emmett-Teller (BET) [33]. The term "modified" in BET isotherm means that the model has been derived from its original form to properly applicable in the liquid-solid system. This is because the conventional BET isotherm [34] requires one to define the saturation pressure which is only valid for the gas-solid system.

The approach for a solution in the two-parameter model was done using linear regression while for the three-parameter model using non-linear regression. The Langmuir and modified-BET models are expressed in Eq. (2.7) and (2.8), respectively.

$$q_e = q_m \frac{K_{Lm} C_e}{1 + K_{Lm} C_e} \tag{2.7}$$

$$q_e = q_m \frac{K_S C_e}{(1 - K_L C_e)(1 - K_L C_e + K_S C_e)} \tag{2.8}$$

where K_{Lm} is Langmuir adsorption isotherm constant in L/mol, K_S is the equilibrium constant of adsorption for BET first-site in L/mol, K_L is the equilibrium constant of adsorption for upper sites in L /mol, and q_m adsorption capacity of adsorbent in mol/g. The optimized parameters of those models are given in Table 2.3.

We have seen from the adsorption kinetics analysis that Cs^+ was chemisorbed on sorption sites of the calcium silicate insulator material. The nature of the interaction was further analyzed through the two isotherms with and without the presence of competing ion Na^+. If such inferred dependency was incorrect, then there should be no effect before and after introducing Na^+ to the solution and only one isotherm model would be necessary to explain them.

Table 2.3 Estimated parameters of adsorption isotherm models.

Sample	Langmuir isotherm model		Modified BET isotherm model		
	K_{Lm} (L/mol)	q_m (mol/g)	K_S (L/mol)	K_L (L/mol)	q_m (mol/g)
Calcium silicate	8.9	0.047	11	0.38	0.061

In fact, as presented in Fig. 2.6, the Langmuir model was only applicable in our study with Na^+ while modified-BET only for that without Na^+ because each model represented different phenomenon as sorbate concentration increased. Without Na^+, three distinctive processes become apparent as a function of Cs^+ concentration: the dashed red line represents the dominant adsorption process is surface complexation; the solid red line represents surface site saturation; the dash-dot red line represents surface precipitation [35,36]. On the other hand, when Na^+ was introduced to the solution, the selectivity adsorption of sorbent (calcium silicate) occurred between Na^+ and Cs^+ [32,37,38] which in turn could decrease the activity of Cs^+ and available adsorption sites.

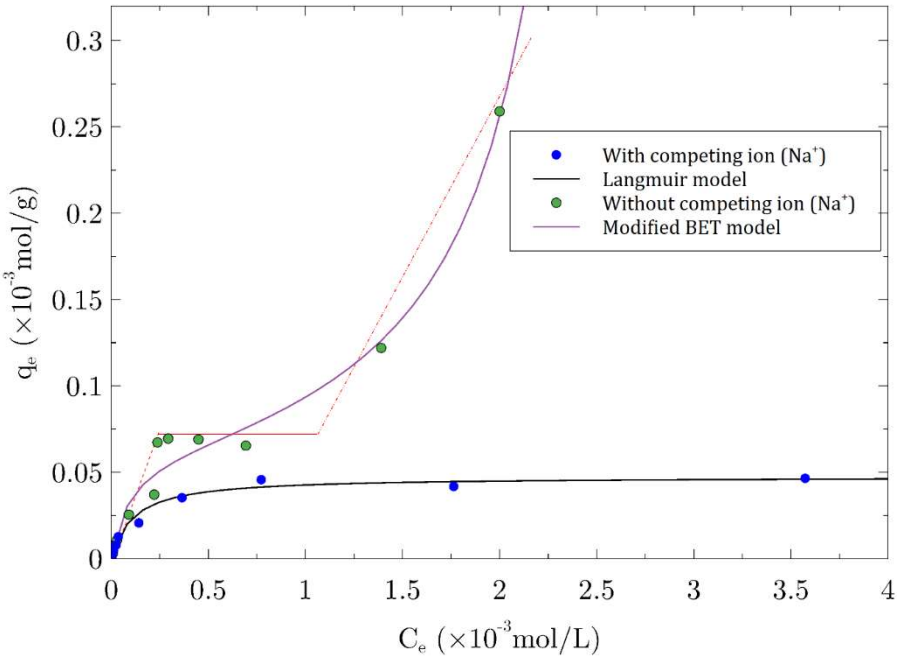

Fig. 2.6 Adsorption isotherm results of calcium silicate as function of cesium concentration under the effect of competing ion in the aqueous solution (Cs loading: 1.3×10^{-6}–3.5×10^{-3} M; Na loading: 0.01 M; adsorbent concentration: 1 g/L; temperature: 25°C, contact time: 98 hours).

This could be deduced on the results where surface precipitation was hindered, and the adsorption capacity was reduced from 0.061 mmol/g to 0.047 mmol/g. These effects could also be explained by the fact that Na^+ competed for the sorption with Cs^+ or screened the negative electrostatic potential of the sorbent and diminished the favorable interaction with Cs^+.

2.7 FTIR analysis

The procedure that had been performed in this analysis was arranged in accordance to rule out the possibility of cesium physically adsorbed on calcium silicate. The samples from the adsorption isotherm experiments without Na^+ were used so that we could obtain the nature of adsorption in this material. Three samples were selected based on the observed phenomenon (i.e., surface complexation, surface site saturation, and surface precipitation) and one sample without Cs intake. Here, after completing the procedure (as described in subchapter 2.3.4), only the higher binding energy between sorbate and sorbent would withstand which is chemisorption. Therefore, the change of respective vibrational modes in FTIR analysis after those procedures will represent such a sorption process.

The nature of vibrational mode in this calcium silicate insulator material is the characteristic of its predominant chemical compound, xonotlite. There are three groups of vibration bands in this material: the first group is due to CO_3^{2-} vibration, the second group is due to bending and stretching vibrations of water molecules and O–H groups, and the third group is silicate tetrahedral vibrations [39]. Among these groups of the bands, we observed the shift of vibrational mode occurred by the interaction with Cs^+ on the silicate tetrahedral second intense

absorption with the wavenumber of 550–400 cm^{-1}. This is the O–Si–O deformation or bending mode [39–41].

Initially, in the sample without Cs loading, this mode had a sharp peak at 462 cm^{-1} and a shoulder at 456 cm^{-1} (black line), which the absorbance intensity difference between them about 60%. Upon Cs loading, the peak and shoulder intensity behaved differently. At the Cs loading of 4.0×10^{-5} M (i.e., condition of surface complexation) the peak intensity was reduced and slightly shifted to 463 cm^{-1} while the shoulder intensity increased. This was caused by Cs^{+} occupancy on the active sites which could inhibit the bending or deformation vibrations of O–Si–O and yielded lower intensity than that of without Cs loading. As the Cs loading attained saturation on 3.1×10^{-4} M which completely occupied all the active sites, the peak on 463 cm^{-1} was undetectable and only the previous shoulder remained on 456 cm^{-1}. At last, when the Cs loading increased to 2.3×10^{-3} M (the condition of surface precipitation), the shoulder turned as the new peak at 458 cm^{-1}. The new observed peak at 458 cm^{-1} has signified the formation of a surface phase whose composition varies between that of the original solid and a pure precipitate of sorbate [35].

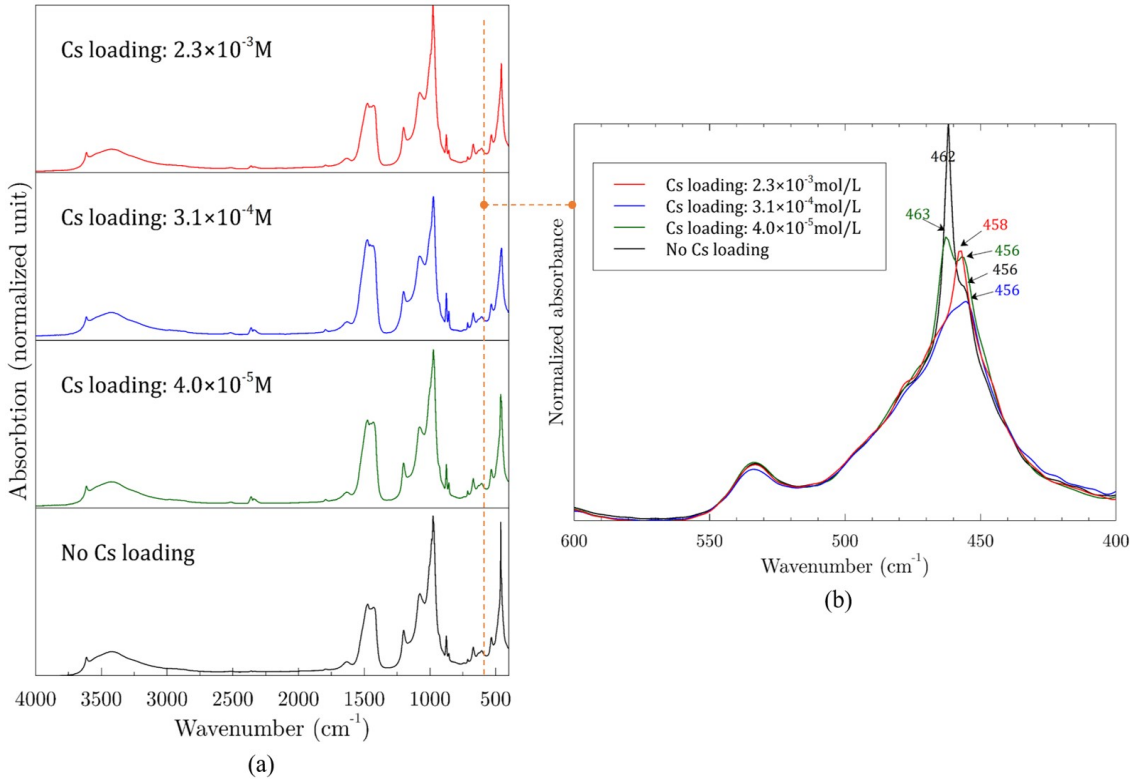

Fig. 2.7 FTIR results of calcium silicate insulator material: (a) 4000–400 cm^{-1}; (b) enlarged graph on 600–400 cm^{-1}.

Indeed, the formation would involve coordination between silicate and Cs but to some extent, the exact compound and how it occurred couldn't be unveiled by infrared spectroscopy. Thus, some proper underlying investigation measures are required in the future, for instance, unveiling the local structure of materials by the extended X-ray absorption fine structure (EXAFS) which has been demonstrated by Schlegel et al [19] when investigating Eu(III) uptake on calcium silicate hydrate (i.e., in which one of the samples was Ca/Si: 1). They interpreted the results that the coordination of Eu(III) occurred by the replacement of Ca^{2+}

in the Ca layer and the interlayer leading to the formation of C–S–H-like solid phase (surface precipitate).

2.8 Chapter summary

Room-temperature adsorption behavior of cesium on a calcium silicate insulation material predominantly composed of xonotlite ($Ca_6Si_6O_{17}(OH)_2$) was studied by analyzing the adsorption kinetics, isotherm, and the infrared spectroscopy. The adsorption kinetics showed that the adsorption process of cesium followed the pseudo-second order reaction model that highly indicated chemisorption of cesium. Equilibrium of adsorption was achieved within 24 hours for the low adsorbent concentration (1 g/L) and 98 hours for the high concentration (5 g/L). To further unveil the sorption process, the adsorption isotherms were obtained with and without the competing Na^+ ion in aqueous solutions. The data were represented well with the Langmuir isotherm model in the presence of Na^+ while the modified Brunauer-Emmett-Teller isotherm model fitted well to that without Na^+. This clearly showed that the adsorption process was altered where surface sites became limited or favorable interaction was screened by Na^+, and the formation of surface precipitates were hindered. The FTIR spectroscopy provided supporting evidence for such sorption that the vibrational peak of O–Si–O deformation or bending mode was attenuated and

shifted from 462 to 458 cm^{-1} as a result of the formation of surface complexes and precipitates.

Chapter 3 Thermochemical analysis of calcium silicate insulator material and cesium hydroxide

3.1 Objectives of this chapter

The purposes of the chapter are to investigate the reaction temperature of interaction between cesium hydroxide with calcium silicate that subjected to temperature increase and under influences of oxidizing and reducing atmosphere conditions, and to characterize the end-products of such an interaction.

3.2 Brief overview of the chapter

Unlike the previous chapter that dealing with room-temperature experimentation in the solid-liquid system, the present chapter is presented in the effort to study the phenomenon of calcium silicate–cesium interaction at high-temperature condition, where the concern system is solid-gas interaction. Before advancing to realize the aforementioned interaction, it necessitates an information about reaction temperature because at the location where Author presumed interaction occurred (i.e., piping systems of the main steam line) the temperature might vary from 403 K to 1103 K [42]. Considering this wide temperature range, the analysis is initially devoted to obtaining the actual reaction temperature and

then proceed to emulate the condition at that obtained temperature. In doing so, a method called thermogravimetry-differential thermal analysis (TG-DTA) was performed, where involving a solid-solid system. The analysis was performed from room temperature condition where calcium silicate insulator material and cesium hydroxide are in the solid phase.

The thermogravimetry-differential thermal analysis is in the class of thermal analysis which involves the measurement of certain physical and chemical properties as a function of temperature. The basic technique for thermogravimetry is to record the mass of a sample as a function of temperature or time, while differential thermal analysis measures the temperature difference between a sample and an inert reference material as a function of temperature [43]. The combination of both methods enables one to analyze thermal events in the sample which do or do not involve mass change. Figure 3.1 illustrates typical thermal analysis involving those two methods in which the sample and the reference material are subjected to constant heat rate. As the sample is subjected to temperature rise, the corresponding material in this sample becomes affected. The example given here shows the sample firstly experiences large endothermic reaction and then followed by small exothermic reactions. Some processes such as

dehydration, melting, or polymorphic transition could be as the event of interest, and explaining the event would require thorough analyses.

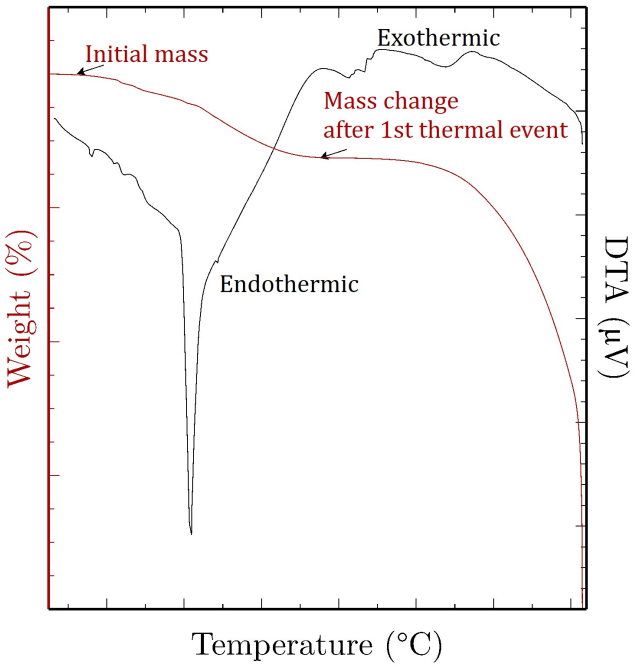

Fig. 3.1 Typical TG-DTA curves.

3.3 Experimental

3.3.1 Materials

Two types of calcium silicate insulation materials were prepared. A calcium silicate insulation powder that was obtained by pulverizing a calcium silicate (hereinafter referred to calsil, to distinguish it with the rest of calcium silicates) insulation block (i.e., manufactured sample following JIS A9510 No.1-15 Standard). The other calsil—with the intention of evaluating the chemical

reaction owing to change of its initial crystal phase—was obtained by pre-heating the pulverized calsil under the condition described later, hereinafter referred to pre-heat treated calsil (PHT calsil). The reagent-grade cesium hydroxide monohydrate, $CsOH \bullet H_2O$ (Sigma Aldrich, 99.5%) was used as a cesium source. A reagent-grade $CaSiO_3$ (Sigma Aldrich, 99%) was used in the separate heating tests as a benchmark for the calcium silicate insulator material.

3.3.2. Characterization

An electric furnace was used for preparing PHT calsil at the pressure of 0.1MPaG in platinum crucible under Ar-5%H_2 constant flow of 200 cm^3/min and maximum temperature of 950°C. A coupled thermogravimetry-differential thermal analysis (TG-DTA, Thermo plus EVO2/TG-DTA 8121, Rigaku) was used to analyze thermal events in the samples which being heated in platinum crucible at pressure of 0.1MPaG under Ar-5%H_2 and Ar-4%H_2-20%H_2O constant flow of 200 cm^3/min and a heating rate of 10°C/min from about 25°C to 1100°C. The retention time at maximum temperature for all samples is one minute unless otherwise specified.

X-ray diffraction (XRD) analyses were performed at room temperature to identify crystal phases of samples after TG-DTA using Rigaku MiniFlex600SC (600 W, Cu Kα radiation). The scan range was 2θ = 10–60° with a continuous

mode in a scan speed of 1°/min and step of 0.01°. The applied current and voltage were 15 mA and 40 kV, respectively. Field emission scanning electron microscopy equipped with energy dispersive X-ray spectrometry (SEM/EDS, JSM-7610F, JEOL) were utilized to characterize the morphology changes and elemental distributions in the samples. A double-sided carbon tape was affixed on Al sample holder to place the samples and without any further coating. The secondary electron images were obtained at the applied voltage of 15 kV. Elemental composition was quantitatively analyzed using a sequential X-ray fluorescence spectrometer (XRF-1800, Shimadzu) with Rh target at the applied voltage and current of 40 kV and 95 mA, respectively and the scan speed of 4°/min. All experimental conditions are summarized in Table 3.1.

3.3.3 Sample preparation

3.3.3.1 Calsil mixed with cesium hydroxide (CsOH)

Calcium silicate (calsil) insulator material and CsOH were mixed with an agate mortar and pestle in the glove box under nitrogen gas flow to prevent CsOH reaction with moisture. Calsil ($Ca_6Si_6O_{17}(OH)_2$) with 81.0 wt% and $CsOH \bullet H_2O$ powders 19.0 wt% were mixed to provide molar ratio of Cs/Ca approximately equal to one. The mixed powder was pressed into the disc-shaped mold with a diameter of 3 or 5 mm for the TG-DTA analyses.

Table 3.1 List of samples and the experimental condition for chemical reaction test of calcium silicate (calsil) insulation and cesium hydroxide.

Sample ID.	Sample name	Initial mass (mg)	Atmosphere	Temp. (°C)	XRD	SEM/ EDS
T1	$CsOH \bullet H_2O$	36.6	Ar-5%H_2	700	—	—
S1	Calsil	177	Ar-5%H_2	950	○	○
S2	PHT calsil	88.5	Ar-4%H_2-20%H_2O	1100	—	—
S3	PHT calsil+$CsOH \bullet H_2O$	23.1	Ar-5%H_2	700	○	—
S4	PHT calsil+$CsOH \bullet H_2O$	16.5	Ar-5%H_2	1100	—	—
S5	PHT calsil+$CsOH \bullet H_2O$	176	Ar-4%H_2-20%H_2O	1100	○	○
S6	Calsil+$CsOH \bullet H_2O$	32.3	Ar-5%H_2	575	○	—
S7	Calsil+$CsOH \bullet H_2O$	45.4	Ar-5%H_2	1100	○	—
S8	Calsil+$CsOH \bullet H_2O$	118	Ar-5%H_2	1100	○	○
S9	Calsil+$CsOH \bullet H_2O$	67.8	Ar-5%H_2	730 #	○	—
S10	Calsil+$CsOH \bullet H_2O$	26.8	Ar-4%H_2-20%H_2O	1100	○	—
S11	Calsil+$CsOH \bullet H_2O$	27.0	Ar-5%H_2	1100	—	—
S12	Calsil+$CsOH \bullet H_2O$	67.4	Ar-4%H_2-20%H_2O	1100	○	—
S13	PHT calsil+$CsOH \bullet H_2O$	21.7	Ar-4%H_2-20%H_2O	1100	○	—
S14	PHT calsil+$CsOH \bullet H_2O$	95.1	Ar-4%H_2-20%H_2O	1100	○	—
B1	$CaSiO_3$	47.0	Ar-5%H_2	1100	○	○
B2	$CaSiO_3$+$CsOH \bullet H_2O$	70.5	Ar-5%H_2	1100	○	○
B3	$CaSiO_3$+$CsOH \bullet H_2O$	77.7	Ar-5%H_2-20%H_2O	1100	○	○

○: examined in SEM/EDS or XRD; #: 10-minute retention time

3.3.3.2 Pre-heat treated calsil (PHT calsil) mixed with cesium hydroxide

For a fundamental study on the interaction of cesium with calcium silicate insulation, the calsil was pre-heat treated (PHT calsil). It is accounted as the evaluation on the possibility of this material firstly interacts with its high-temperature atmosphere in the real installation site of the primary piping system of nuclear power station before its interaction with cesium.

In order to produce a larger amount of the PHT calsil sample, the calsil powder was heat-treated inside an electric furnace with the platinum crucible. The XRD analysis was performed after the heat treatment, which mainly identified wollastonite ($CaSiO_3$) as the main constituent of the PHT calsil—where larnite (Ca_2SiO_4) also being identified as a minor compound—as shown in Fig 3.2. Figure 3.3 depicts the micrograph of calsil and PHT calsil, respectively.

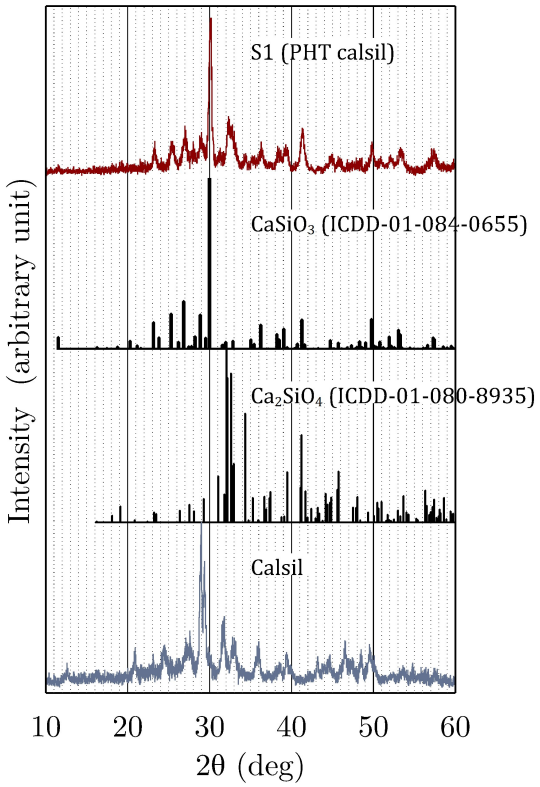

Fig 3.2 XRD pattern of pre-heat treated calcium silicate insulation (PHT calsil) and calsil.

Fibers included in calsil were decomposed and broken in PHT calsil sample. Then, after those characterizations, the sample was mixed with CsOH in a similar way to calsil. PHT calsil with 40.9 wt% and $CsOH \bullet H_2O$ with 59.1 wt% were mixed to provide molar ratio of Cs/Ca approximately equal to one. After mixing, samples were also pressed into the disc-shaped mold with a diameter of 3 or 5 mm.

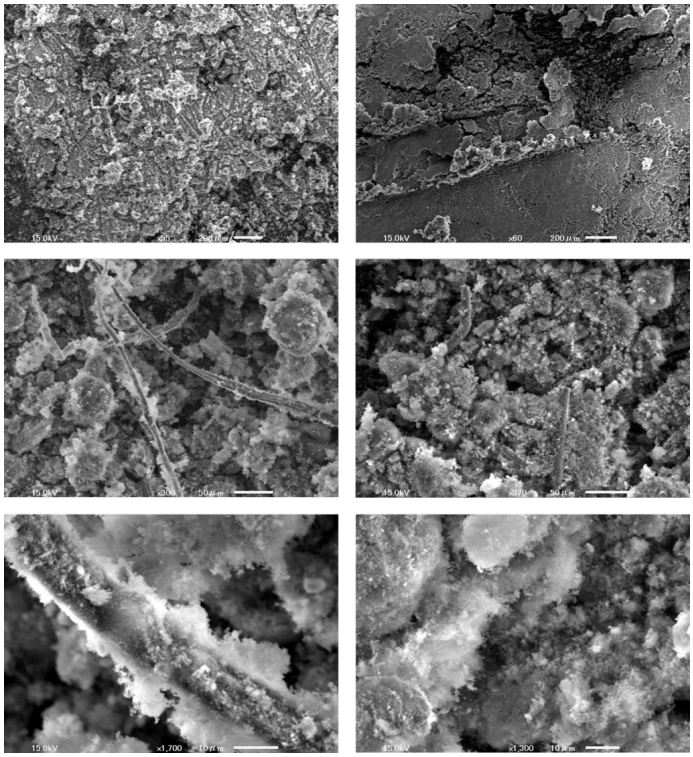

Fig 3.3 Secondary electron image of (left) calsil and (right) PHT calsil. PHT calsil was identified as wollastonite ($CaSiO_3$) crystal while calsil was composed of predominant xonotlite ($Ca_6Si_6O_{17}(OH)_2$) and minor tobermorite ($Ca_5Si_6O_{16}(OH)_2 \bullet 4H_2O$).

3.4 Effect of atmospheric condition on calsil: pre- and post-mixing with cesium hydroxide

3.4.1 Pre-heat treated calsil

The results of TG-DTA analysis, as presented in Fig. 3.4 for calsil which undergoes heat treatment (i.e. to form heat-treated calsil) under Ar-5%H_2 and

Ar-4%H_2-20%H_2O conditions show similar thermal event and volatile materials in the calsil are almost completely vaporized up to around 700°C regardless of oxidizing or reducing condition. Above this temperature, two small exothermic reactions are observed. They are associated with (1) loss of remaining hydroxyls and (2) xonotlite ($Ca_6Si_6O_{17}(OH)_2$) and/or tobermorite ($Ca_5Si_6O_{16}(OH)_2 \bullet 4H_2O$) transformation to wollastonite ($CaSiO_3$) [44-46].

It should be emphasized that the sample in our study was a product of hydrothermal reaction (CaO-SiO-H_2O) which at last consisted of mixed xonotlite and tobermorite while those employed in the reported works [44-46] were distinctive/separate experiments on xonotlite and tobermorite. Thus, the second loss of remaining hydroxyls that was observed in our sample around 720°C, was not observed by those works. Nevertheless, the onset of transformation into wollastonite (800°C) in our study was in agreement with those reports.

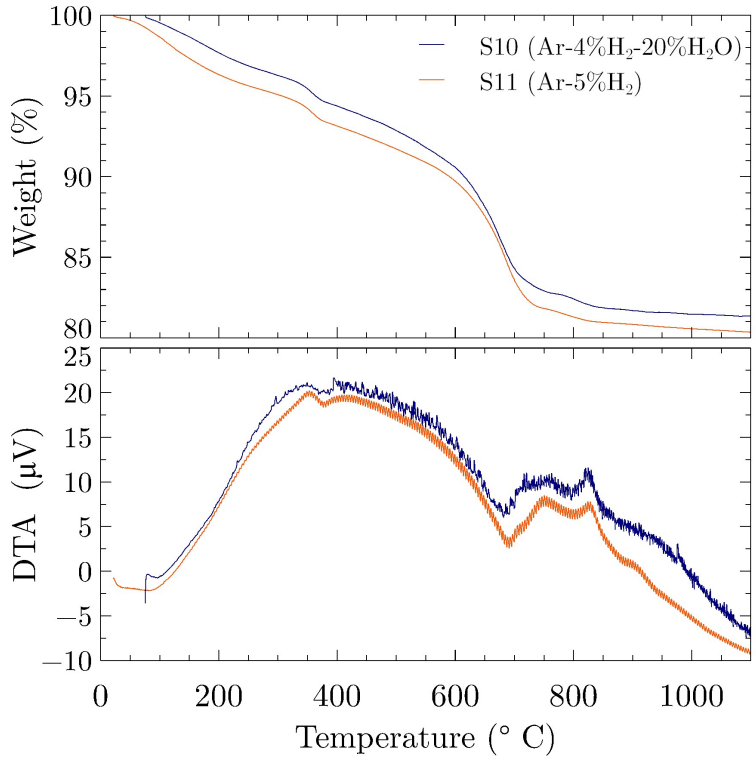

Fig. 3.4 TG-DTA curves of calsil under heat treatment in Ar-5%H_2 and Ar-4%H_2-20%H_2O with maximum temperature of 1100°C.

3.4.2 Pre-heat treated calsil mixed with cesium hydroxide

Figures 3.5 shows the TG-DTA curves under Ar-5%H_2 condition for PHT calsil mixed with $CsOH \bullet H_2O$ (S3, S4) and $CsOH \bullet H_2O$ (T1). Sharp endothermic reaction around 200°C in our samples resulted from the melting of $CsOH \bullet H_2O$ (refer to the phase diagram of CsOH-H_2O system reported by Liljenzin and Schock [47]).

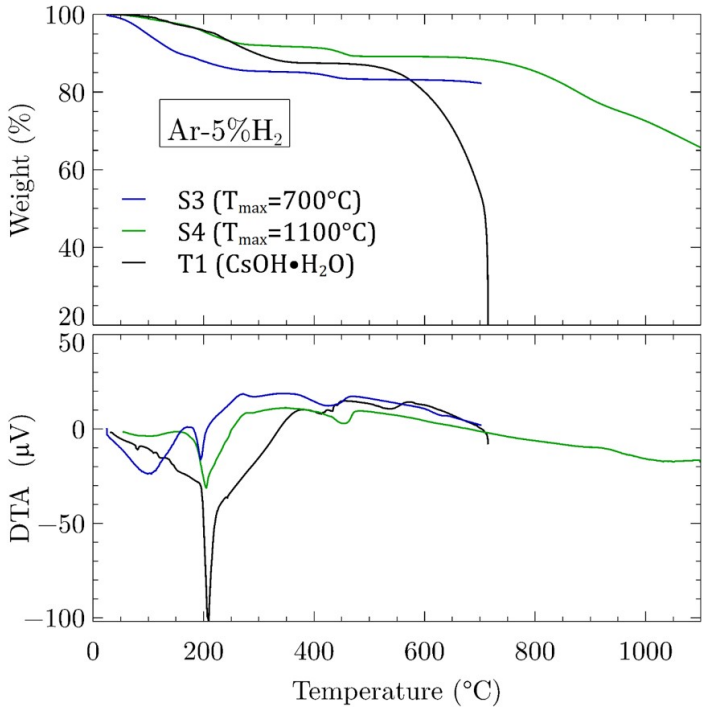

Fig. 3.5 TG-DTA curves of PHT calsil mixed with $CsOH \bullet H_2O$ in different temperature limit under Ar-5%H_2 atmosphere and curve for non-mixing $CsOH \bullet H_2O$.

Small endothermic reaction and weight loss at the temperature beyond 400°C appeared simultaneously, while no weight loss at the same temperature was observed for $CsOH \bullet H_2O$ (T1). Furthermore, there was no change in DTA curves above 500°C and the weight loss started around 700°C. Then, to examine whether interaction occurred at such a temperature range, the mixed sample (S3) which being heated up to 700°C was examined by XRD. No cesium compounds were present, and the XRD pattern of S3 almost similar to that of PHT calsil or

$CaSiO_3$, in Fig. 3.6. Thus, the endothermic reaction at the temperature beyond 400°C is not related to a chemical reaction between PHT calsil and CsOH although—in the case of Ar-4%H_2-20%H_2O—a similar diffraction pattern appeared and the interaction between PHT calsil and CsOH was identified.

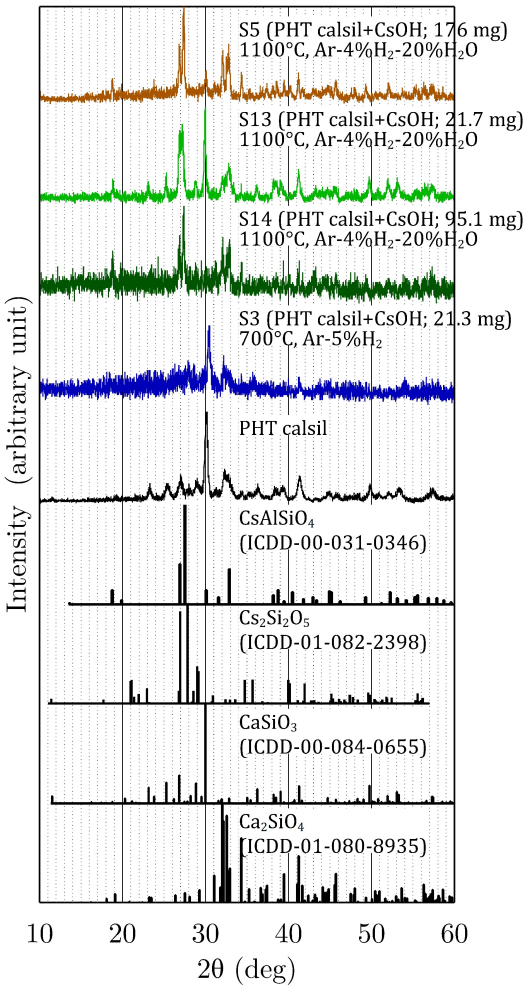

Fig 3.6. XRD patterns of PHT calsil mixed with $CsOH \bullet H_2O$ after subjected to heat treatment up to 1100°C under Ar-5%H_2 and Ar-4%H_2-20%H_2O, and the attribution to PHT calsil, $CaSiO_3$, Ca_2SiO_4, $Cs_2Si_2O_5$, and $CsAlSiO_4$.

Figures 3.7 describes the TG-DTA curves of PHT calsil mixed CsOH and non-mixed PHT calsil (S5, S13, S14, S2), which were heated under Ar-4%H_2-20%H_2O. The sharp endothermic reaction around 200°C observed in the case of Ar-5%H_2 disappeared; a gradual endothermic appeared at temperature lower than 200°C under Ar-4%H_2-20%H_2O.

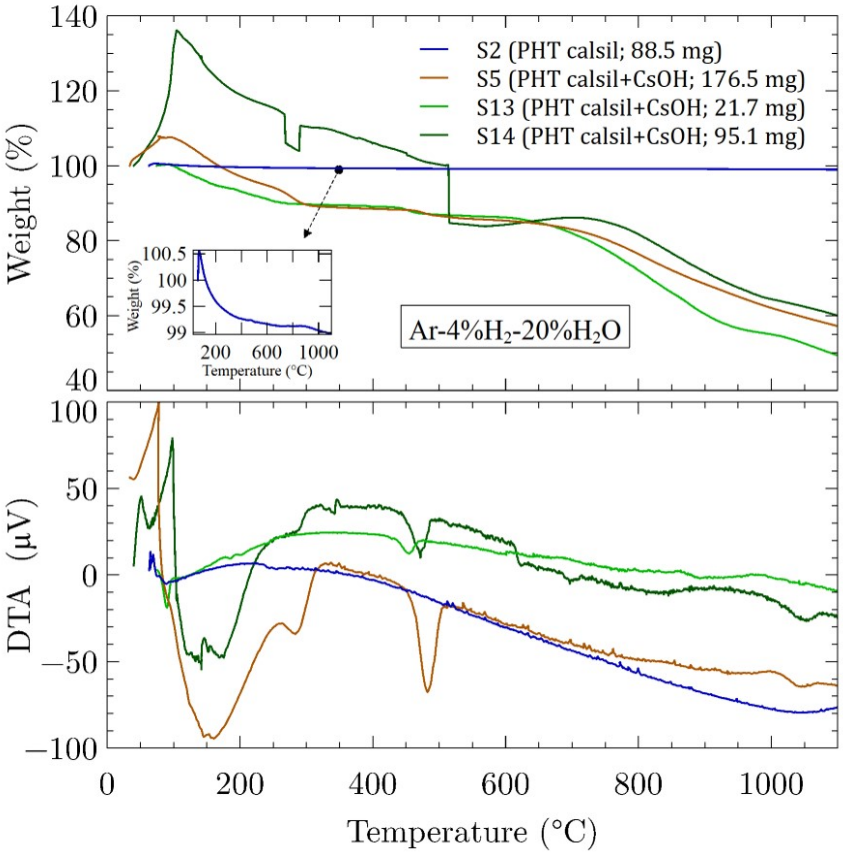

Fig. 3.7 TG-DTA curves of PHT calsil mixed with $CsOH \bullet H_2O$, and PHT calsil (non-mixing sample). Atmospheric condition: 1100°C, Ar-4%H_2-20%H_2O.

In the case of the Ar-4%H_2-20%H_2O condition, according to the phase diagram [47], solid $CsOH \bullet H_2O$ can disappear to become liquid form of CsOH and such a sharp endothermic peak can disappear due to steam partial pressure was greater than 123 mbar (i.e. 20%H_2O corresponds to 200 mbar steam partial pressure). The gradual endothermic below 200°C appeared for the mixed samples (S5, S14), which suggested that steam partial pressure became greater than 123 mbar. In fact, both of the TG curves of S5 and S14 indicated weight gains and suggested that these samples absorbed steam at temperature lower than 200°C. Consequently, the gradual endothermic peak below 200°C has been considered to have resulted from the transition of solid to liquid forms of CsOH, accompanying water absorption.

TG-DTA curves in Ar-4%H_2-20%H_2O in the temperature range from 400°C to 1100°C appeared not to be significantly different from those in Ar-5%H_2 although the endothermic peak intensities at the temperature beyond 400°C became large. The difference in these endothermic peak intensities between Ar-5%H_2 and Ar-4%H_2-20%H_2O is likely caused by an increased amount of loaded sample and enhancement of interaction between PHT calsil and liquid CsOH.

The XRD pattern in Fig. 3.6 indicates that the peak intensities of $CaSiO_3$ for S5 and S14 with larger sample amounts are weaker, compared to that of the

small loaded sample (S13). It was also found that another compound namely cesium aluminum silicate, $CsAlSiO_4$, was identified along with Ca_2SiO_4. This result implies that cesium interacts with PHT calsil. The fact that cesium aluminum silicate was formed instead of cesium silicates (e.g., $Cs_2Si_2O_5$, $Cs_2Si_4O_9$, Cs_6SiO_3) had shown that aluminum, despite the existence as a minor element in calcium silicate with approximate percentage of 0.94% (i.e., the list of respective element percentage is given on Table B.1), played an important role to yield the reaction. The quantitative analysis of sample S5 by using the RIR method in Rigaku integrated X-ray powder diffraction software, PDXL© version 2.7.2.0, shows the amount of Ca_2SiO_4 is 95.9 wt%, followed by $CsAlSiO_4$ with 4.1 wt% (Appendix B, Fig. B.2).

The thermodynamic calculations using thermodynamic data [48–51] were performed to evaluate whether $CaSiO_3$ reacts with CsOH. As a result, two following reactions would likely to occur:

$$4CaSiO_3(s) + 2CsOH(c) = 2Ca_2SiO_4(s) + Cs_2Si_2O_5(s) + H_2O(g) \quad (3.1)$$

$$2CaSiO_3(s) + 2CsOH(c) = Ca_2SiO_4(s) + Cs_2SiO_3(s) + H_2O(g) \quad (3.2)$$

where s means solid phase, c condensed phase, and g gaseous phase. However, the lowest Gibbs free energy of reaction was obtained if alumina included in the system, and $CsAlSiO_4$ could be formed by the following reaction:

$$4CaSiO_3(s) + Al_2O_3(s) + 2CsOH(c) = 2CsAlSiO_4(s) + 2Ca_2SiO_4(s) + H_2O(g). \quad (3.3)$$

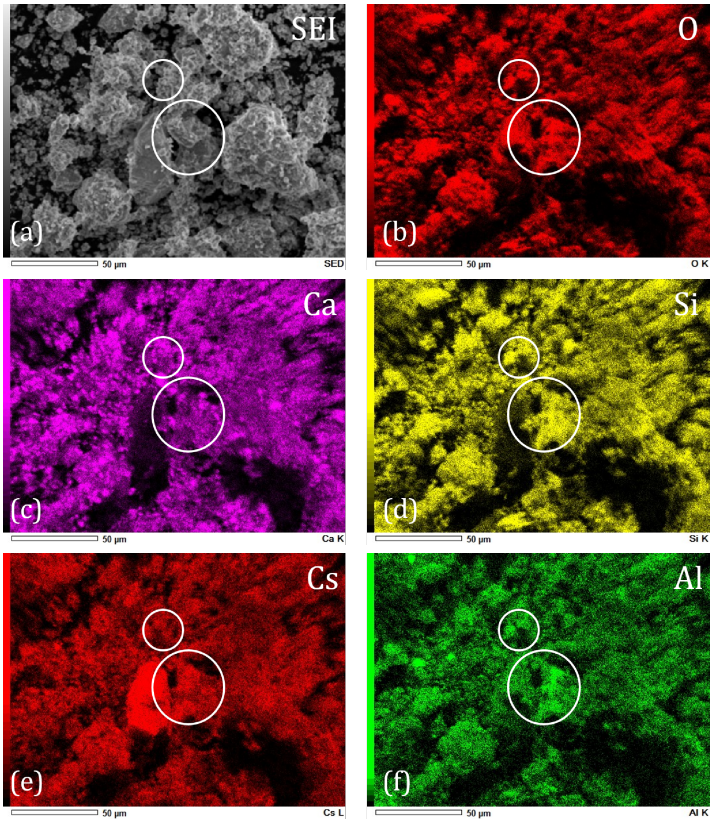

Fig. 3.8 Energy dispersive X-ray spectroscopy (EDS) elements mapping of S5 (PHT calsil + $CsOH \bullet H_2O$ in Ar-4%H_2-20%H_2O heated up to 1100°C). In the circle area, the distribution of Cs is partially coincident with that of O, Si, and Al but not coincident with that of Ca.

The results of SEM/EDS analysis for PHT calsil mixed with $CsOH \bullet H_2O$ in Ar-4%H_2-20%H_2O (S5) are shown in Fig. 3.8. The EDS mapping revealed that the elemental distribution of Cs was congruent with that of Si, O and Al in several

places. Therefore, this EDS result becomes supporting evidence of chemical interaction between PHT calsil and CsOH which forming $CsAlSiO_4$.

The comparison of TG-DTA in Fig. 3.9 signifies no major difference in Ar-5%H_2 and Ar-4%H_2-20%H_2O for PHT calsil mixed with $CsOH \bullet H_2O$ (S4, S5, S13) after being heated above 400°C. However, $CsAlSiO_4$ was not identified in the sample heated below 700°C (S3)—Figure 3.6. Therefore, in the temperature range of 700°C to 1100°C the chemical interaction between PHT calsil and $CsOH \bullet H_2O$ is expected to occur.

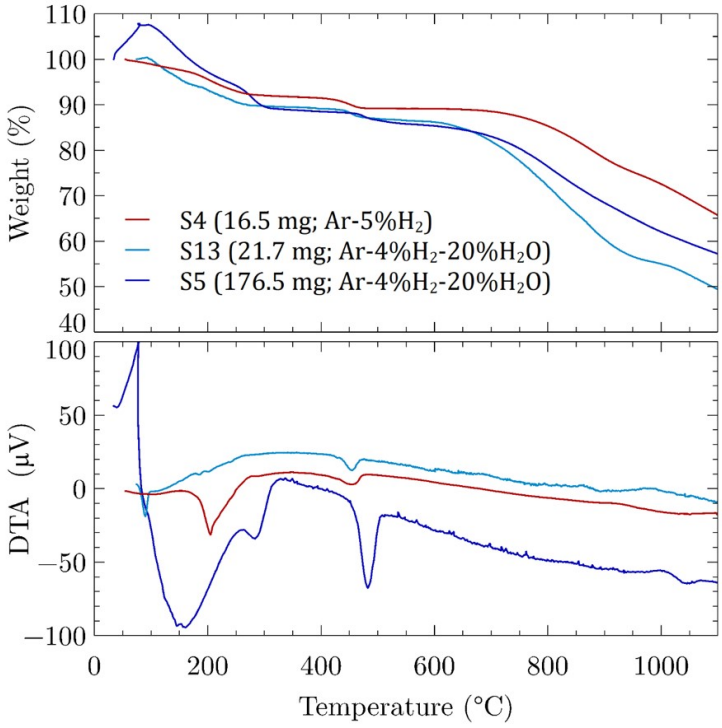

Fig. 3.9 Comparison of TG-DTA curves between Ar-5%H_2 and Ar-4%H_2-20%H_2O atmosphere for PHT calsil mixed with $CsOH \bullet H_2O$.

3.4.3 Calsil mixed with cesium hydroxide

Figure 3.10 presents the results of the TG-DTA curves under Ar-5%H_2 condition for calsil mixed with $CsOH \bullet H_2O$ (S7, S8), together with those for calsil (S11) and $CsOH \bullet H_2O$ (T1). No sharp endothermic peak around 200°C appeared, like the case of PHT calsil in Ar-5%H_2 as shown in Fig. 3.5. However, a similar gradual endothermic at less than 200°C appeared like that in the case of PHT calsil in Ar-4%H_2-20%H_2O (Fig. 3.7).

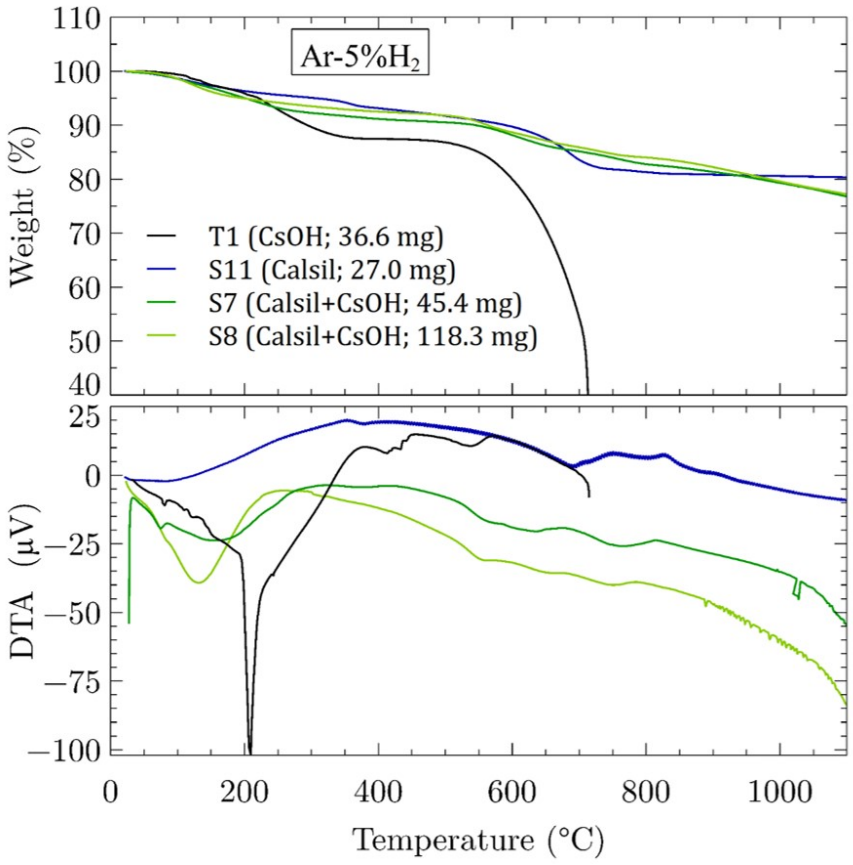

Fig. 3.10 TG-DTA curves of calsil mixed with $CsOH \bullet H_2O$, calsil (non-mixing sample) and $CsOH \bullet H_2O$. Atmospheric condition: 1100°C, Ar-5%H_2.

In other words, a similar atmospheric condition to that the samples under Ar-4%H_2-20%H_2O was realized and a transition from CsOH liquid form to solid $CsOH \bullet H_2O$ would occur with increasing temperature. Some endothermic reactions in the temperature range of 550 to 800°C appeared in contrast to the case of PHT calsil mixed with $CsOH \bullet H_2O$. Thus, to determine the temperature threshold when the chemical interaction occurred, two types of samples were prepared by heating up to 575°C and 730°C, and the resulting compounds were examined by XRD.

The comparison of the XRD analyses for these samples (S6, S9) as well as the samples heated up to 1100°C (S7, S8) is shown in Fig. 3.11. As shown in this figure, $CsAlSiO_4$ presents in the sample heated up to 730°C (S9) but not in that up to 575°C (S6). Therefore, the chemical interaction of calsil mixed with $CsOH \bullet H_2O$ in Ar-5%H_2 occurred in the temperature range of 575°C to 730°C. Both Fig. 3.12 (a) and (b) show the micrograph, and EDS point analysis for calsil mixed with $CsOH \bullet H_2O$ after heated in Ar-5%H_2 (S8). The EDS mapping results (Fig. 3.13) indicated the congruency among Cs, O, Si, Al but not as intense as that in sample S5. This is because —unlike sample S5 where crystal phase of calcium silicate had been changed to wollastonite ($CaSiO_3$) prior to the interaction with CsOH—the process of xonotlite decomposition and transition into

wollastonite occurs concurrently with that of interaction to CsOH to form $CsAlSiO_4$ which in turn causing such effect on elemental distribution.

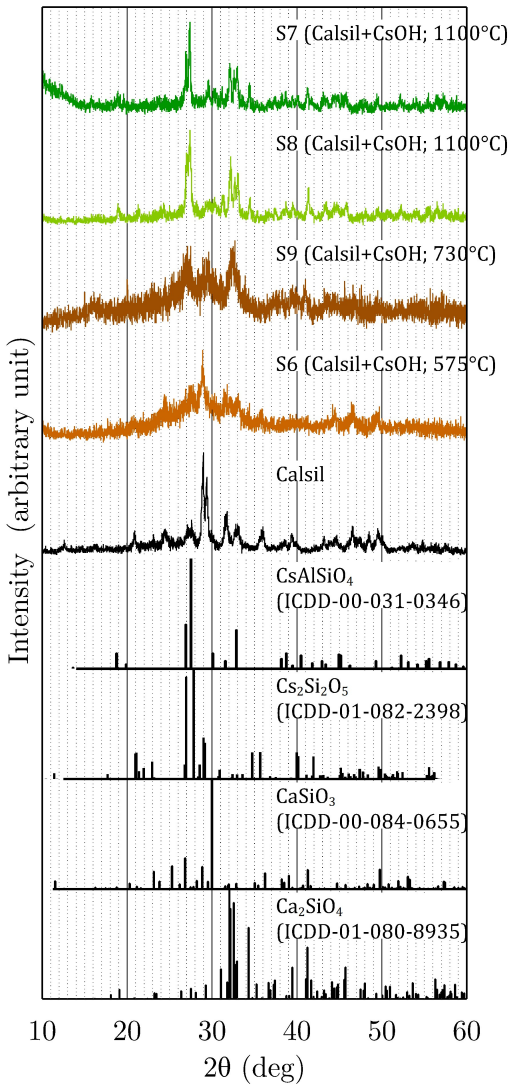

Fig. 3.11 XRD patterns of calsil mixed with $CsOH \bullet H_2O$ after subjected to different temperature limit under Ar-5%H_2, and the attribution to calsil, $CaSiO_3$, Ca_2SiO_4, $Cs_2Si_2O_5$, and $CsAlSiO_4$.

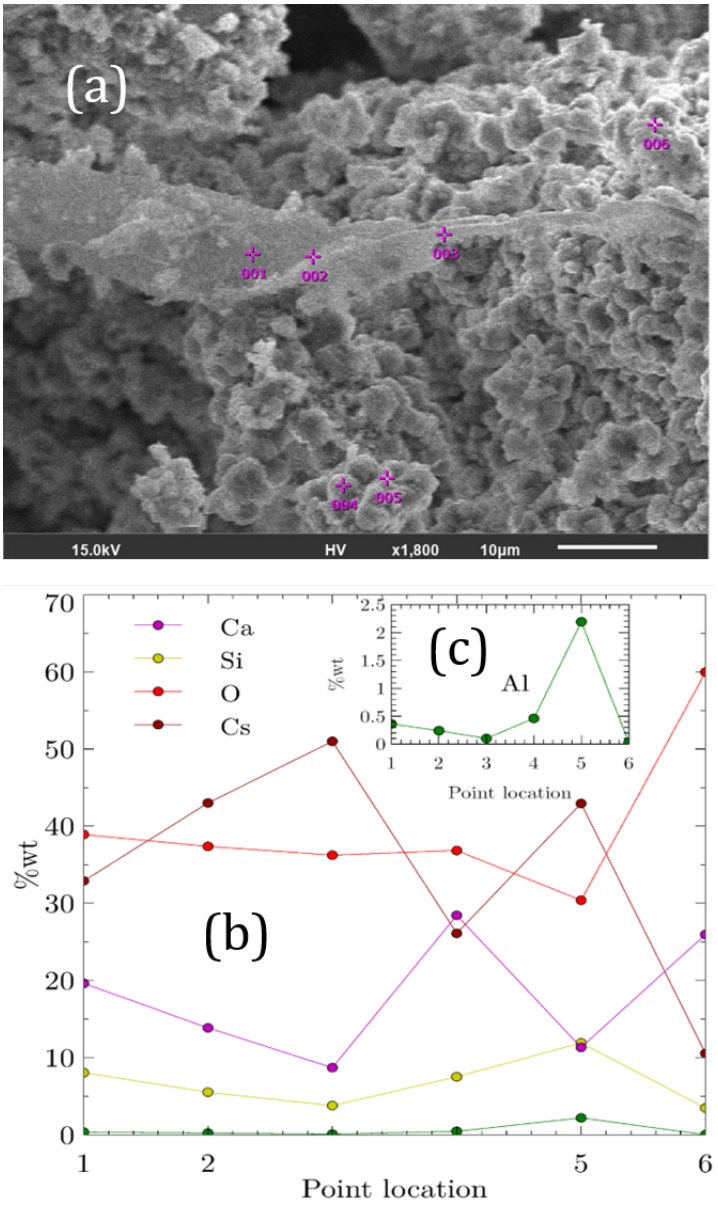

Fig. 3.12 (a) Secondary electron image showing the assigned points for (b), (c) EDS point analysis of S8 (calsil+$CsOH \bullet H_2O$ in Ar-5%H_2 heated up to 1100°C).

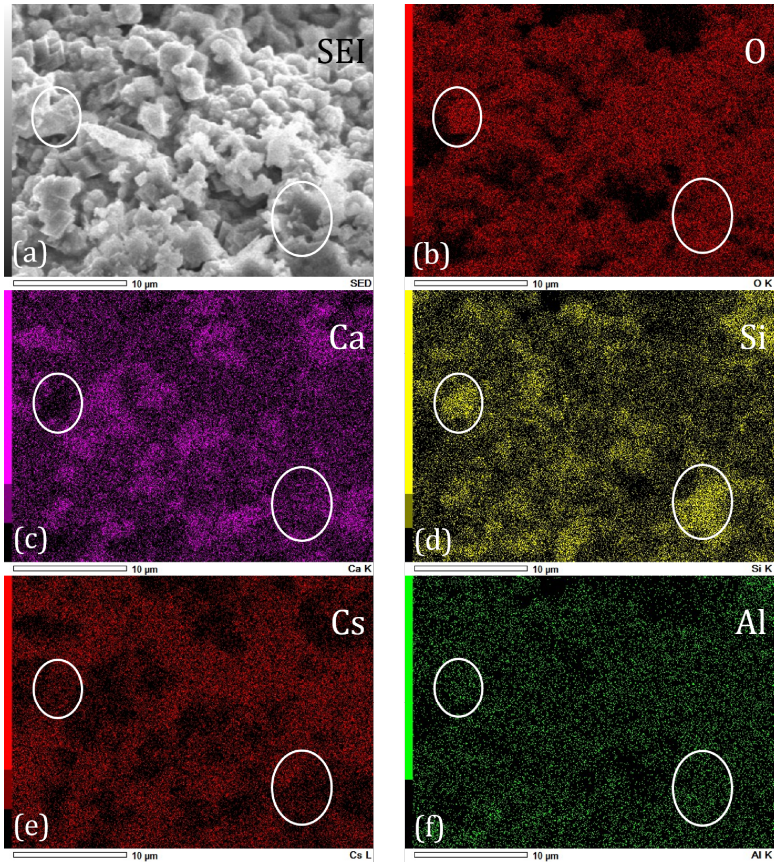

Fig. 3.13 EDS elements mapping of S8 (calsil+$CsOH \bullet H_2O$ in Ar-5%H_2 heated up to 1100°C). Circle area marks the congruency distribution of Cs, O, Si, and Al.

The thermodynamic calculations using thermodynamic data [48–51] were also evaluated. Similar to the case of PHT calsil (i.e. $CaSiO_3$), the reaction with CsOH which forming cesium silicate in the following reactions would likely to occur yet the lowest Gibbs free energy of reaction can be obtained if alumina included in the system (i.e., Eq. 3.6):

$$2Ca_6Si_6O_{17}(OH)_2(s) + 6CsOH(c) = 3Cs_2Si_2O_5(s)$$

$$+ 6Ca_2SiO_4(s) + 5H_2O(g) \quad (3.4)$$

$$Ca_6Si_6O_{17}(OH)_2(s) + 6CsOH(c) = 3Cs_2SiO_3(s)$$

$$+ 3Ca_2SiO_4(s) + 4H_2O(g) \quad (3.5)$$

The formation of $CsAlSiO_4$ is as the following reaction:

$$2Ca_6Si_6O_{17}(OH)_2(s) + 3Al_2O_3(s) + 6CsOH(c) = 6CsAlSiO_4(s)$$

$$+ 6Ca_2SiO_4(s) + 5H_2O(g) \quad (3.6)$$

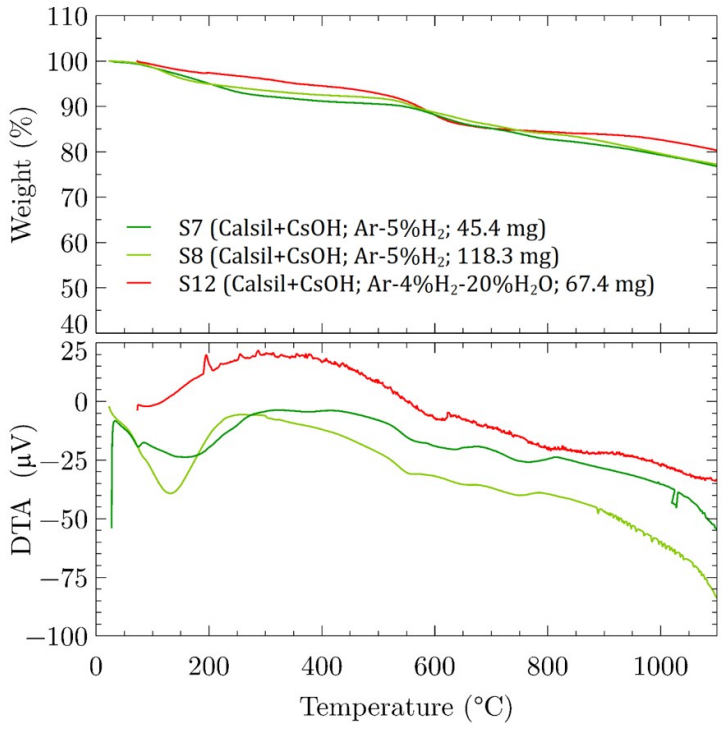

Fig. 3.14 TG-DTA curves comparison between Ar-5%H_2 and Ar-4%H_2-20%H_2O atmosphere for calsil mixed with $CsOH \bullet H_2O$.

The TG-DTA results comparison both heat treatment in Ar-5%H_2 and Ar-4%H_2-20%H_2O atmosphere for calsil mixed with $CsOH \bullet H_2O$ (S7, S8, S12) are presented in Fig. 3.14. The TG-DTA curve in Ar-4%H_2-20%H_2O appears not to be significantly different from that in Ar-5%H_2 except for the DTA curve at temperature lower than 200°C. No endothermic reaction at temperature lower than 200°C might be due to the disappearance of solid $CsOH \bullet H_2O$ and also dehydration of calsil are expected to cause the steam partial pressure greater than 200 mbar (i.e., 20% of H_2O) where solid $CsOH \bullet H_2O$ disappears. The endothermic reaction in the temperature range from 550°C to 800°C for calsil mixed with $CsOH \bullet H_2O$ in Ar-4%H_2-20%H_2O (S12) are weaker than those for the mixed samples in Ar-5%H_2 (S7, S8), although the loaded amount of the mixed sample S12 are larger than that of the mixed sample S7. Furthermore, it was found from the TG curve that the weight loss of the mixed sample S12 was smaller than those of the mixed samples (S7, S8).

3.4.4 Comparison of calsil and pre-heat treated calsil upon mixed with cesium hydroxide

Figure 3.15 and 3.16 show the TG-DTA curves and XRD patterns for both calsil mixed with $CsOH \bullet H_2O$ and PHT calsils mixed with $CsOH \bullet H_2O$, respectively.

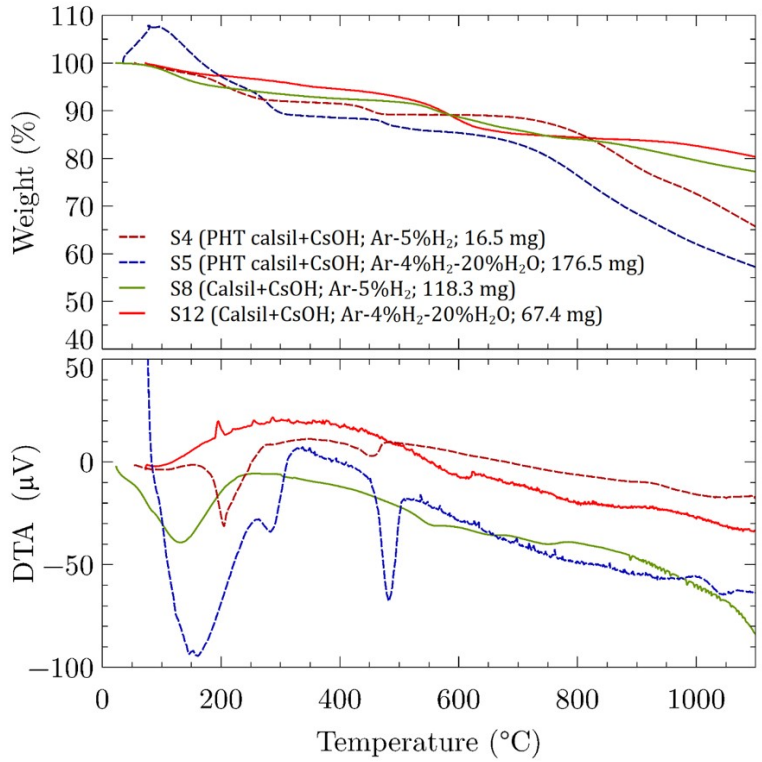

Fig. 3.15 TG-DTA curves comparison of calsil mixed with $CsOH \bullet H_2O$ and PHT calsil mixed with $CsOH \bullet H_2O$ under Ar-5%H_2 and Ar-4%H_2-20%H_2O atmosphere.

The results of the XRD analysis indicate that $CsAlSiO_4$ is formed in both types of calsils heated up to 1100°C although TG-DTA analysis cannot explicitly identify on which temperature range chemical interactions occur between the calsil and CsOH. This could be as a result of coincidence between xonotlite-wollastonite crystal transformation ($Ca_6Si_6O_{17}(OH)_2 \rightarrow CaSiO_3$) and the reaction of $CaSiO_3$ with CsOH.

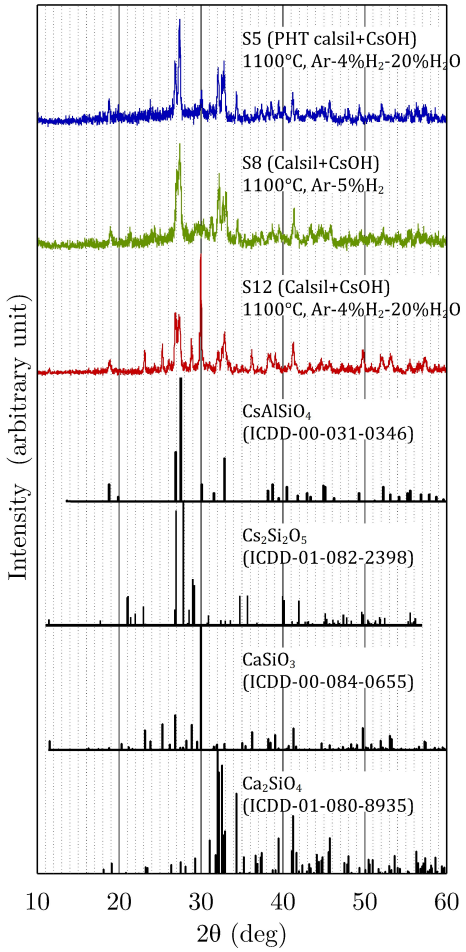

Fig. 3.16 XRD pattern of calsil mixed with $CsOH \bullet H_2O$ and PHT calsil mixed with $CsOH \bullet H_2O$ (after subjected to heat treatment up to 1100°C under Ar-5%H_2 and Ar-4%H_2-20%H_2O), and the attribution to Ca_2SiO_4, $CaSiO_3$, $Cs_2Si_2O_5$, and $CsAlSiO_4$.

The fact is also can be drawn from Fig 3.10 on temperature 550°C to 800°C. A similar but wider exothermic was observed on sample S7 and S8. From the separate experiment (see subchapter 3.4.1), it was suggested that those

exothermic reactions on S11 associated with loss of remaining hydroxyls and recrystallization to $CaSiO_3$.

Two major tasks remain from the analyses of interaction of calsil with cesium hydroxide: (1) The high weight percentage of cesium in EDS point analysis (see Fig. 3.12) and (2) the significance of aluminum (i.e., calsil impurity in 0.94 wt%) to yield the reaction instead of direct reaction with silicates to form cesium silicate. If one combines the two aforementioned conditions, one may raise a question of how such a low content of aluminum in the sample produces approximately 40 wt% of cesium end-product if this resulted from cesium aluminum silicate. Indeed, such an inference would contradict all the facts, and the possibility of a high percentage could be also from the condensed CsOH which did not react with calsil. Therefore, the dissolution process of post-heat treatment samples is taken to eliminate such a possibility and is presented in the next subchapter. Additionally, the reagent-grade $CaSiO_3$ is examined in separate heating test experiments of which mixed with cesium hydroxide and then prior to the characterization, a similar dissolution process is conducted for all samples.

3.5 Effect of dissolution and impurity on the interaction with cesium hydroxide

3.5.1 Effect of dissolution process

As briefly described in the previous subchapter, the given dissolution process here is provided to dissolve the condensed CsOH in the sample so that a more valid representation of the cesium amount in connection with the aluminum distribution. Cesium hydroxide is highly dissolved in water at room temperature of which 300 g/100 g of H_2O [52]. So that using deionized water as the dissolving agent is sufficient in the present study, even though another dissolving technique is feasible such as the one performed by Nishioka et al [53] using aqua regia (i.e., 35 wt% HCl: 60 wt% HNO_3 = 2:1) to remove the water-insoluble Cs deposits from their chemisorbed samples.

Sample S5 (i.e., PHT calsil mixed with CsOH; heat-treated up to 1100°C in Ar-4%H_2-20%H_2O) was used in the dissolving process. Before the heating test, it was known that the amount of $CsOH \bullet H_2O$ was 104 mg (59.1 wt%) and this required at least 100 µL of deionized water to dissolve it. However, considering the matrix of sample being mixed with PHT calsil which could attenuate the dissolution efficiency, 2 mL of H_2O was applied. The sample was soaked in about one hour and separated from the supernatant. Then, the sample was dried using

a ceramic hot plate with the temperature of 110°C for an hour of constant heating time. Upon completing the process, the SEM/EDS and XRD were performed to the sample.

The EDS point analysis of sample S5 after dissolution is given in Fig. 3.17. The amount of cesium is significantly decreased in comparison with the pre-dissolution one. This result could unveil the cause of a high percentage in previous analysis was a result of condensed CsOH being remained in the sample. Hence, the obtained value in the analysis could represent the insoluble Cs compound that has been identified before, namely cesium aluminum silicate. The EDS elemental mapping in Fig. 3.18 describes the congruency among Cs, Al, Si, O but not Ca.

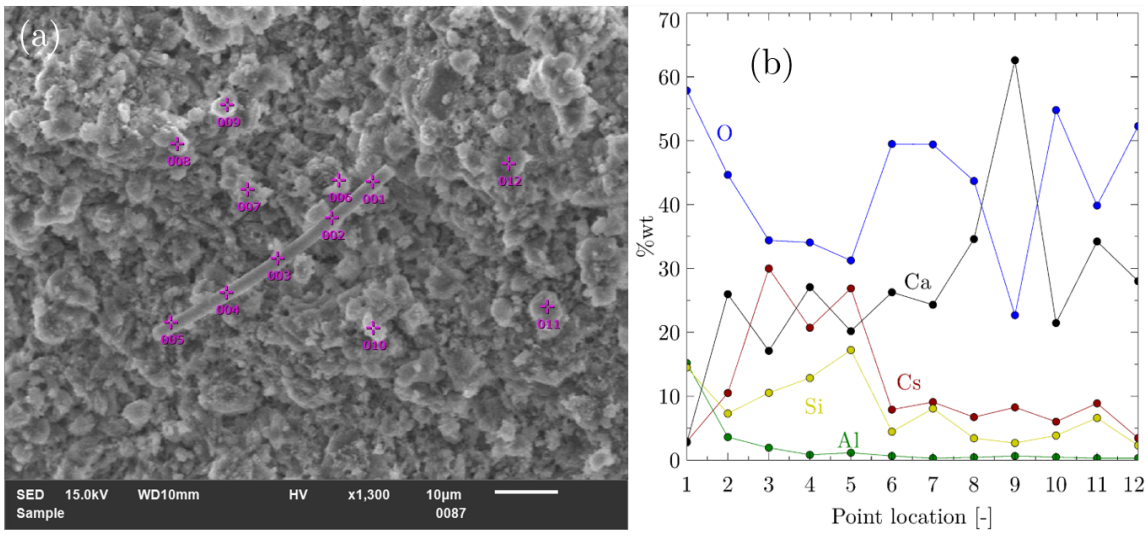

Fig. 3.17 (a) Secondary electron image showing assigned points for (b) EDS point analysis of S5 after the dissolution.

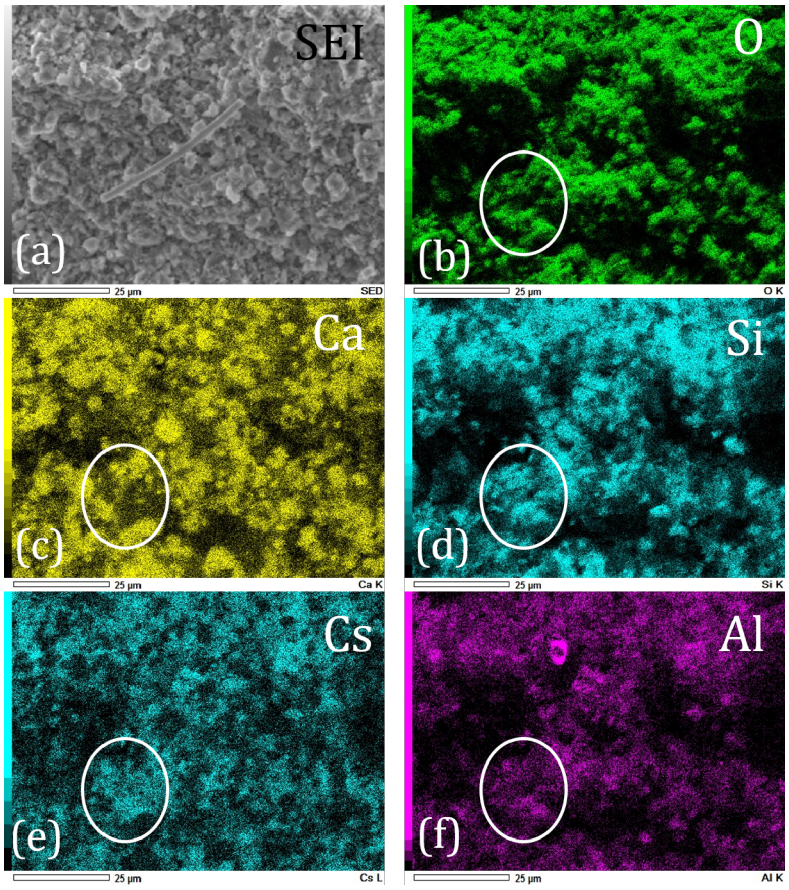

Fig. 3.18 EDS elements mapping of S5 after dissolution. Circle area marks the congruency distribution of Cs, O, Si, and Al.

Despite the suggested cesium aluminum silicate formation by EDS elemental mapping in the post-dissolution sample, it is imperative to validate the result through crystal phase identification using XRD analysis. The results of XRD patterns comparison for PHT calsils mixed with $CsOH \bullet H_2O$ pre- and post-dissolution are shown in Fig. 3.19. The characteristic diffraction of which previously being identified as $CsAlSiO_4$ in pre-dissolution remains in the post-

dissolution sample. This implies that the cesium compound in the end-product is stable and water-insoluble.

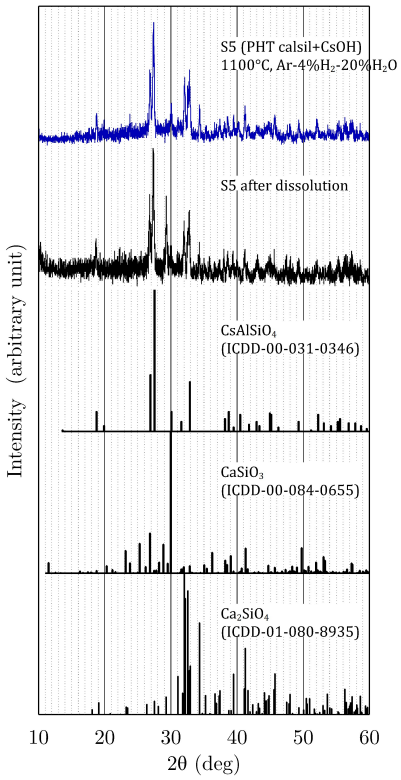

Fig. 3.19 XRD patterns of S5 before and after dissolution, and the attribution to Ca_2SiO_4, $CaSiO_3$, and $CsAlSiO_4$.

3.5.2 Effect of impurity

A high purity reagent grade calcium silicate, $CaSiO_3$, was purchased from Sigma Aldrich (Sigma Aldrich, 99%) for the heating test with cesium hydroxide. This is imperative and would be the core evidence because the major findings described in previous subchapters have been concentrated on the formation of new cesium compound in calcium silicates (i.e., calsil and PHT calsil) which

involves the presence of aluminum as the impurity. Before advancing to the heating test, the elemental analysis of the reagent using SEM/EDS was performed and presented in Fig. 3.20 and Table 3.2.

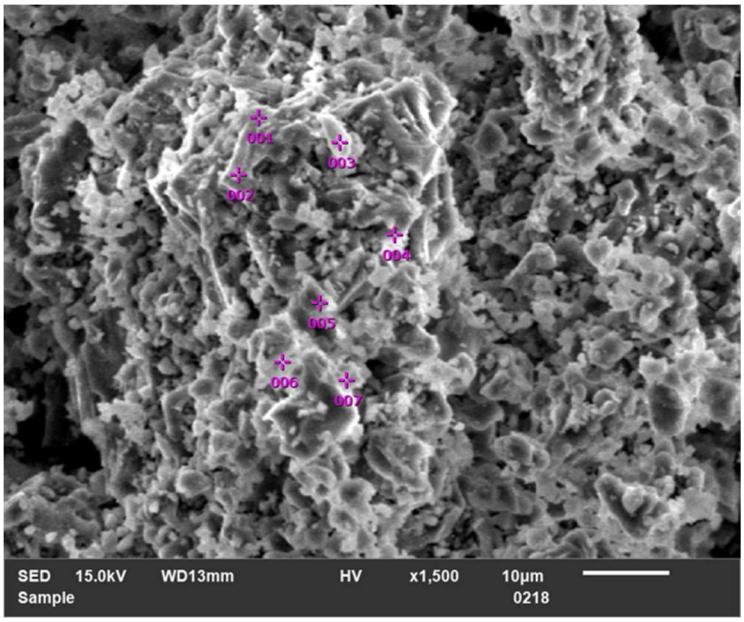

Fig. 3.20 Secondary electron image of reagent-grade $CaSiO_3$.

Table 3.2 Ca/Si atomic ratio and Al weight percentage in the $CaSiO_3$ reagent.

Point location [-]	Ca/Si atomic ratio [-]	Al (wt%)
001	0.943	0.06
002	1.03	0.19
003	0.974	0.08
004	1.93	0.14
005	1.02	0.19
006	1.13	0.17
007	0.913	0.24

Even though the sample is high purity reagent grade, a relatively small amount of aluminum still could be detected in the results of EDS point analysis to which the highest obtained value is 0.24 wt%. This could be resulted from (1) the nature of $CaSiO_3$ starting material of quartz flour and quicklime which could contain alumina regardless of the purification process to be applied and (2) the background electron scattering of the sample holder which is made of aluminum. Nevertheless, it is worth to proceed with the benchmark test considering the value is still comparably 4 times lower than that of calsils (i.e., 0.94 wt%).

The procedure of sample mixing follows the preceding one in subchapter 3.3.3 hence it would not be repeated here. The similar heating test conditions were also applied to avoid the vague results which including the crucible type, atmosphere, flow rate, heating rate, and holding time at maximum temperature. There were three conditions in the heating tests (see Table 3.1): (1) the heating test of reagent without CsOH in Ar-5%H_2 atmosphere and temperature up to 1100°C; (2) with CsOH in Ar-5%H_2 atmosphere and temperature up to 1100°C; (3) with CsOH in Ar-4%H_2-20%H_2O atmosphere and temperature up to 1100°C. After the heating tests, the procedure of dissolution was also conducted on all samples and then followed by crystal phase identification using XRD and elemental analysis using SEM/EDS.

The TG-DTA curves for all three samples are presented in Fig. 3.21. Sample B1, which contains no CsOH, has no weight loss during the heat treatment. This is because the crystal of $CaSiO_3$ in the reagent has no remaining hydroxyls to be decomposed which previously occurred in calsil or PHT calsil. On the other hand, weight changes and several thermal events appear in sample B2 and B3 which contain CsOH.

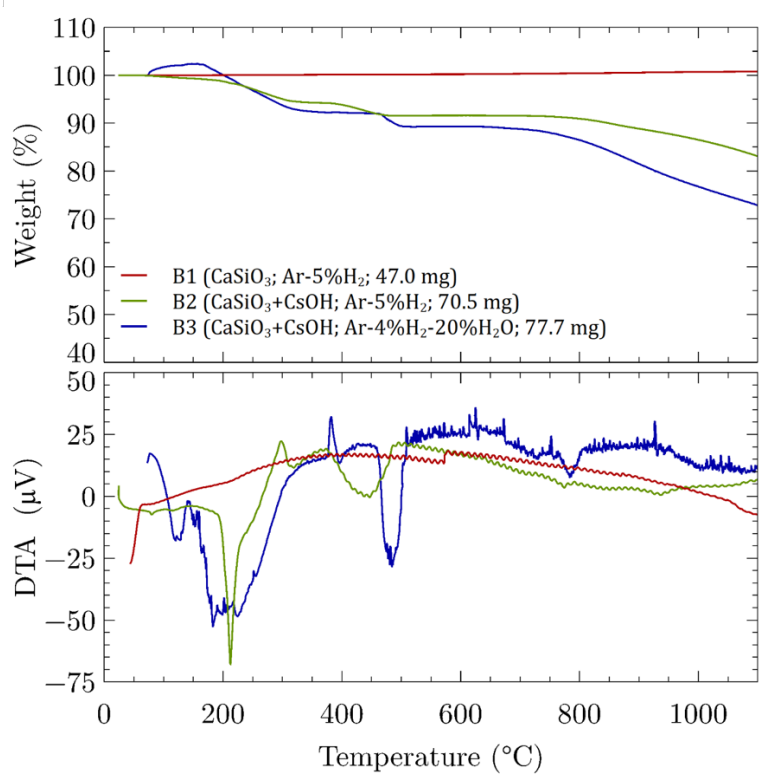

Fig. 3.21 TG-DTA curves of $CaSiO_3$ (non-mixing sample) and $CaSiO_3$ mixed with $CsOH \bullet H_2O$. Atmospheric condition: temperature up to 1100°C, Ar-5%H_2 and Ar-4%H_2-20%H_2O.

At the temperature of 200°C, the thermal events both in Ar-5%H_2 and Ar-4%H_2-20%H_2O are—understood from PHT calsil mixed CsOH heating tests and CsOH phase diagram [47]—related to melting temperature of CsOH for sample in Ar-5%H_2 atmosphere and transition from solid to liquid forms of $CsOH \bullet H_2O$ that accompanying water absorption for sample in Ar-4%H_2-20%H_2O atmosphere. The subsequent thermal events occur as exothermic reaction at temperature range of 282–310°C (B2) and 373–394°C (B3) with no weight loss and endothermic reactions at temperature range of 375–486°C (B2) and 456–512°C (B3) with approximately 3 % weight loss in both cases. The thermal events could be in two plausible causes: First, they could be all accounted for CsOH comprising phase transition and evaporated from sample matrix without any interaction with $CaSiO_3$; second, they are accounted to the interaction of CsOH with $CaSiO_3$ and resulted in end-product possessing different chemical compound. Therefore, the chemical phase identification was done to assess them.

Figure 3.22 gives the XRD patterns comparison for all samples of the reagent (B1, B2, and B3) after the dissolution process, along with the XRD pattern of PHT calsil mixed with CsOH (i.e., where $CsAlSiO_4$, $CaSiO_3$, and Ca_2SiO_4 crystal phases were identified after the heating test). The sample B1 has

exactly the same crystal phase with the reagent before heat treatment, which in agreement with the TG-DTA results (Fig. 3.21) that showing no changes.

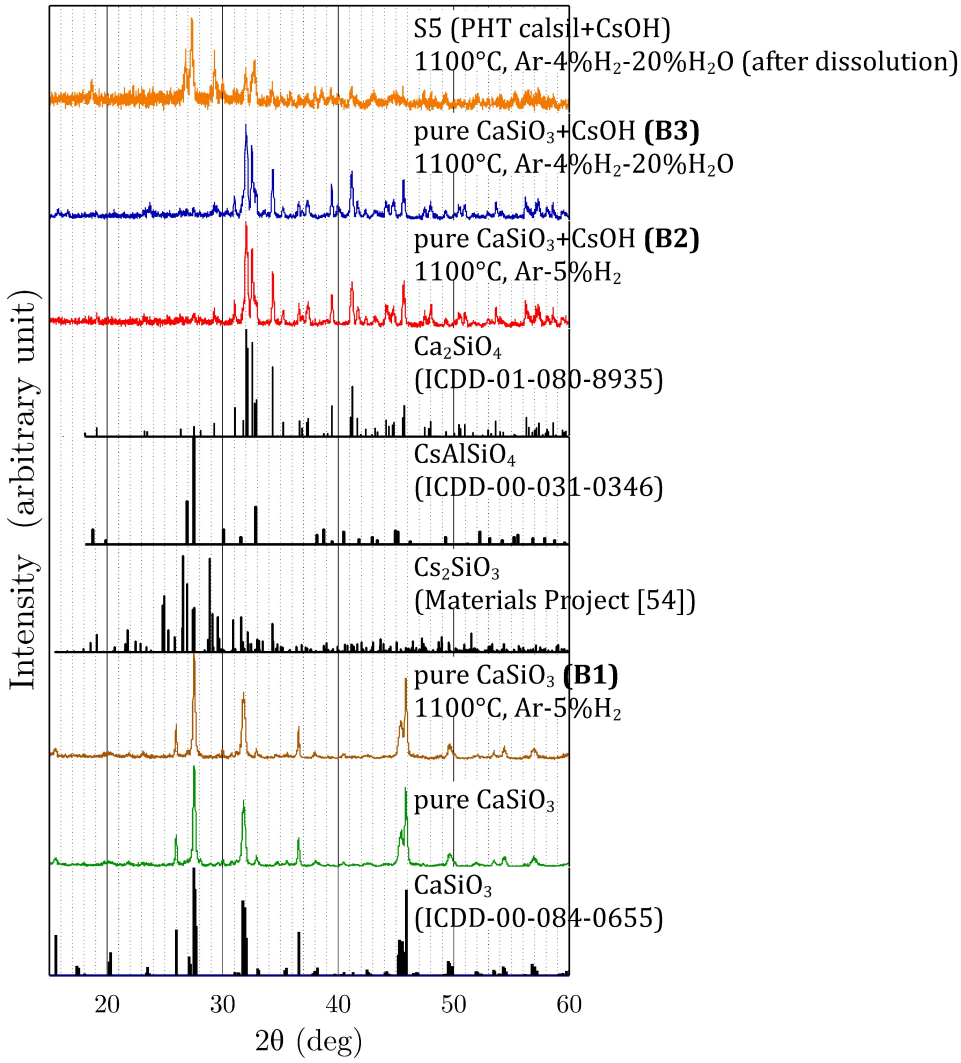

Fig. 3.22 XRD patterns of the high purity reagent mixed and non-mixed CsOH after heating tests, S5 (PHT calsil mixed with CsOH), and the attribution to $CaSiO_3$, Ca_2SiO_4, $CsAlSiO_4$, Cs_2SiO_3.

For both samples B2 and B3, the crystal phase is changed from its original of $CaSiO_3$ to Ca_2SiO_4 and **no $CsAlSiO_4$ being identified**. Hence, the observed thermal events in the TG-DTA clearly result from the phase change to Ca_2SiO_4. This means that the sample regardless of the atmosphere, which is $CaSiO_3$ requires another source of Ca in an equal amount to be thermodynamically valid.

The following thermodynamics calculations using the thermodynamics data [48,50,51] were done by considering the thermal events in TG-DTA:

$$CaSiO_3(s) + 2CsOH(c) = Cs_2SiO_3(s) + CaO(s) + H_2O(g) \quad (3.7)$$

$$CaSiO_3(s) + CaO(s) = Ca_2SiO_4(s) \quad (3.8)$$

Summation of Eqs. (3.7) and (3.8) yields

$$2CaSiO_3(s) + 2CsOH(c) = Cs_2SiO_3(s) + Ca_2SiO_4(s) + H_2O(g) \quad (3.9)$$

It is known that the molar ratio of Ca/Cs prior to heating tests equal to unity. Upon advancing the reaction 3.7, there will be left one mol of $CaSiO_3$ and subsequently reacts with the first reaction product CaO. Therefore, both $CaSiO_3$ and CaO are in an equal amount when forming the Ca_2SiO_4. Also, based on the calculation Cs_2SiO_3 should also be obtained in the end-product crystal phase. In fact, Cs_2SiO_3 can't be identified—using XRD database of Materials Project [54] due to no available data from ICDD (The International Centre for Diffraction

Data). This implies that the Cs_2SiO_3 is water-soluble since the X-ray diffraction was performed after the dissolution or the formed compound has an amorphous structure. If the compound is amorphous, then the formation can be traced by EDS elemental mapping.

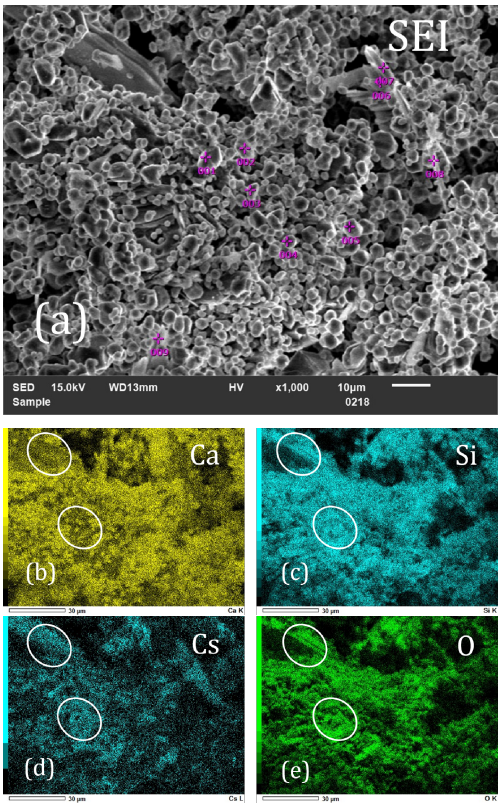

Fig. 3.23 EDS mapping of sample B2 and the assigned point analysis.

Table. 3.3 EDS point analysis of sample B2.

Elements	Molar ratio at point [-]								
	1	2	3	4	5	6	7	8	9
Ca/Si	2.05	1.93	1.97	1.95	1.96	1.42	1.15	7.68	1.62
Cs/Si	0.031	0.0077	0.012	0.027	0.0028	0.25	0.16	0.44	0.38

Figure 3.23 and Table 3.3 provide the EDS elemental mapping and point analysis. The obtained congruency among Cs, Si, and O signifies the aforementioned formation of Cs_2SiO_3, even though the Cs/Si molar ratio is not equal to two. This is because the Si intensity during the analysis is also reflected from another compound that possesses Si, Ca_2SiO_4, to which can be explicitly comprehended from points 1 to 5.

The results of these benchmark heating tests using high purity reagent $CaSiO_3$ have proved the previous findings in PHT calsil (i.e., crystal phase: $CaSiO_3$) and calsil (i.e., crystal phase: $Ca_6Si_6O_{17}(OH)_2$) that indeed formation of new cesium compound in those calcium silicates–which did not suffer the water dissolution–involved aluminum as the minor element. Nevertheless, there should exist a threshold of aluminum inclusion (wt%) in calcium silicate that could yield the reaction with cesium hydroxide and would require an expensive purification technique to do so. Reflecting the fact that majority of calsil products used inside thermal power station in Japan particularly nuclear industry are manufactured in accordance to the same Japanese Industrial Standard (i.e., JIS A9510 No.1-15) [55]–[59], so that such a threshold investigation would not necessary in the present circumstance. However, to elaborate on the prevalence of cesium hydroxide interaction with calcium silicate insulator materials, in the next chapter of this

Doctoral thesis the gas-solid interaction would incorporate other calcium silicates from different manufacturers.

3.6 Chapter summary

The chemical reaction temperature between calcium silicate insulator material (calsil) and cesium hydroxide (CsOH) was experimentally investigated under Ar-5%H_2 and Ar-4%H_2-20%H_2O atmosphere with temperature up to 1100°C. Two types of pre-conditioned calcium silicate insulation materials led to distinct reaction temperature with CsOH: 575°C to 730°C for calsil while 700°C to 1100°C for PHT calsil. Despite of the reaction temperature and difference in initial chemical compounds (calsil: $Ca_6Si_6O_{17}(OH)_2$; PHT calsil: $CaSiO_3$), the end product of those calsils after subjected to reaction with CsOH in temperature up to 1100°C yielded similar XRD pattern regardless the atmosphere condition, which corresponded to the formation of cesium aluminum silicate: $CsAlSiO_4$. Elemental distribution analyses of Cs, Si, O, and Al have revealed the congruent distribution in samples after the experiment to signify the formation. The benchmark heating tests using high purity reagent grade $CaSiO_3$ were supplemented to the analyses to prove the previous findings in calsil and PHT calsil that the formed cesium compound was cesium aluminum silicate. The results have proved that such a cesium aluminum silicate was not formed in all

benchmark samples but in turn yielding the Cs water-soluble compound and Ca_2SiO_4.

Chapter 4 High temperature interaction of cesium hydroxide with calcium silicate insulator materials

4.1 Objective of this chapter

The purpose of this chapter is to investigate the interaction between cesium hydroxide with calcium silicate insulator materials at the reaction temperature obtained from the thermochemical investigation in the previous chapter. The difference with the preceding one, this chapter emulates the real case where cesium hydroxide is transported by high-temperature steam (superheated condition) toward solid calcium silicate insulation block and the post-interaction samples are subjected to crystallographic, elemental, vibrational and morphological analyses.

4.2 Brief overview of the chapter

The present chapter is the last part of this doctoral thesis where the interaction between cesium hydroxide and calcium silicate insulator material is emulated through high temperature steam transport. We have confirmed in the thermochemical investigation that calsil interacted with cesium hydroxide and yielding cesium aluminum silicate ($CsAlSiO_4$) and larnite (Ca_2SiO_4). Nevertheless,

it should be highlighted that both calsil and cesium hydroxide had been made in contact (i.e., mixed using agate mortar) during the heating test that making the probability of interaction high. In contrast—to emphasize the importance of this chapter—the present experimentation would involve high-temperature horizontal furnace where cesium hydroxide and calcium silicate (calsil) being in different locations. Cesium hydroxide is placed on the upstream furnace and transported by steam flow to the downstream furnace in which calsils are located. Two other calsils from different manufacturers are used in this experiment as well as the calsil used in TG-DTA. After accomplishing the experiment, the similar characterization procedures in Chapter 3 are utilized along with infrared spectroscopy.

4.3 Experimental

4.3.1 Materials

Three calcium silicate insulator materials were used in block form. They are the calcium silicate used in the thermochemical investigation (i.e., which previously called as calsil), the calcium silicate from Nippon Keical, Ltd (hereinafter called as NKL calsil), and the calcium silicate from Japan Insulation Co., Ltd (further called as JIC calsil). As the aluminum weight percentage is of the concern, the information was obtained before the experiment for both NKL

calsil (i.e., Al: 0.78 wt%[*]) and JIC calsil (i.e., Al: 0.78 wt%[**]). The reagent-grade cesium hydroxide monohydrate, $CsOH \bullet H_2O$ (Sigma Aldrich, 99.5%) was used as a cesium source.

4.3.2. Characterization

X-ray diffraction (XRD) analyses were performed at room temperature to identify crystal phases of samples after gas-solid interaction tests using Rigaku MiniFlex600SC (600 W, Cu Kα radiation). The scan range was 2θ = 10–60° with the continuous mode in a scan speed of 1°/min and step of 0.01°. The applied voltage and current were 40 kV and 15 mA, respectively. To characterize the morphology changes and elemental distributions in the samples, a field emission scanning electron microscopy equipped with energy dispersive X-ray spectrometry (SEM/EDS, JSM-7610F, JEOL) was utilized. A double-sided carbon tape was affixed on Al sample holder to place the respective samples and without any further coating. The secondary electron images were obtained at an applied voltage of 15 kV. The functional group of the material was analyzed with Fourier transform infrared spectrometry (FTIR, Shimadzu FTIR-8400) by the KBr pellet

[*] Undisclosed private correspondence about XRF result with the company

[**] Deducted from similar Al distribution of EDS point analysis with NKL calsil; the magnitude might be overestimated.

method. Prior to the characterization, all samples were water-dissolved in a similar way as previously performed in Chapter 3.

4.3.3 Gas-solid interaction test facility

The gas-solid interaction test facility used in this study is the research property of Japan Atomic Energy Agency-JAEA ([53], [60]), therefore only some parts of the facility will be described in general way to prevent the copyrights infringement. The facility is comprised of three main parts (in subsequent order): (1) the water tank, (2) the CREST (Chemical REaction with STeel) furnace, and (3) quadrupole mass spectrometer. The steam atmosphere in the furnace is realized by introducing Ar-5%H_2 into the constant temperature water tank. The furnace is 1 meter in length, and consisting of two concentric tubes. At the inner tube with a diameter of 25.4 mm, the upstream is a part of the furnace designated for cesium hydroxide vaporization while the downstream is the location of the samples (in this case for calsils) where the center-to-center distance between them is 355 mm. The concentration of hydrogen and steam at the outlet of the furnace is monitored continuously by the quadrupole mass spectrometer.

4.3.4 Experimental method

Initially, all calsils in the blockish form were cut into the size of 5×5×1 mm using a micro-cutting machine and measured their respective weight before placed into the Ni sample holder/crucible. The CsOH, on the other hand, was prepared inside the glovebox with constant Ar flow to prevent moisture absorption and weighted along with the platinum crucible. After the samples and CsOH preparation, both crucibles were inserted into the furnace and located as previously described in subchapter 4.3.3. Figure 4.1 shows the arrangement of those samples and CsOH as well as the configuration of the gas-solid interaction test facility.

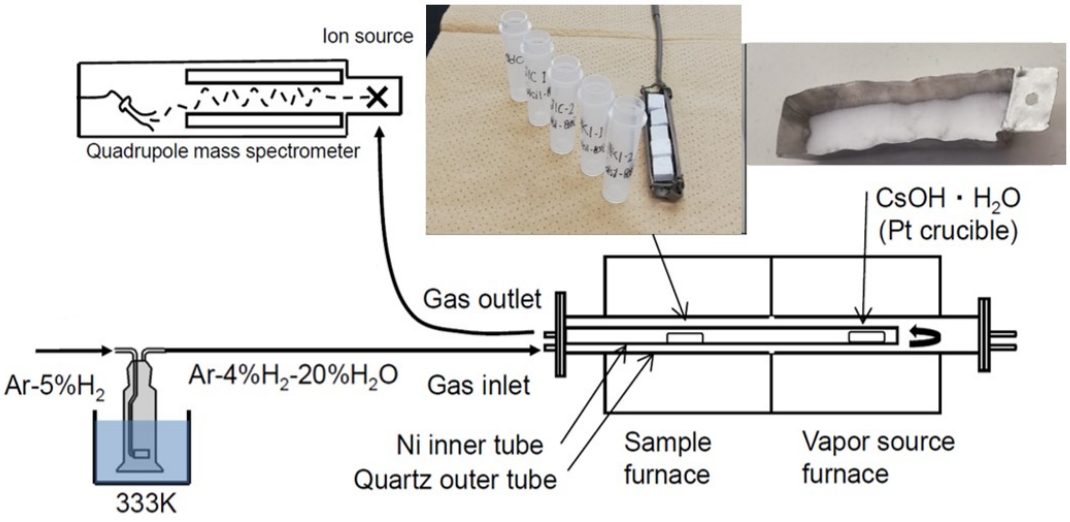

Fig. 4.1 Gas-solid interaction test facility showing calsils (calsil, JIC calsil, NKL calsil) and CsOH allocated part in the furnace.

The order of samples in the Ni crucible (i.e., from upstream to downstream) was arbitrarily chosen and might be interchangeable in any preferred order. The calsil was placed in the upstream part of the sample crucible, followed by JIC calsils (i.e., labeled as JIC calsil-1 and JIC calsil-2) and NKL calsils (i.e., labeled as NKL calsil-1 and NKL calsil-2). After the settlement of samples and CsOH had been done, the furnace was initially degassed to remove the air before starting to introduce the Ar-4%H_2-20%H_2O atmosphere with a flow rate of 100 cm^3/min and pressure of 0.1MPaG.

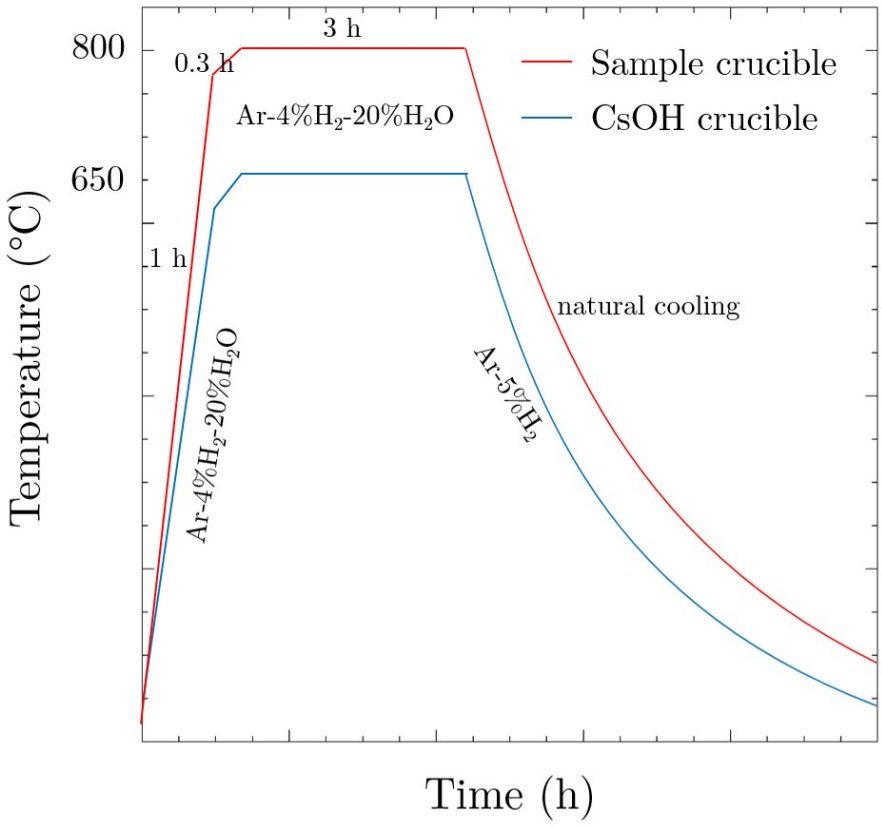

Fig. 4.2 The applied heating and cooling process in gas-solid interaction test.

The schematic diagram in Fig. 4.2 shows the heating and cooling processes for both sample furnace and CsOH furnace as well as the atmosphere at the designated timing. The temperature of 800°C was used based on the previous thermochemical investigation that at this temperature the interaction took place.

The holding time at the maximum temperature was chosen three hours to ensure the complete volatilization of cesium hydroxide [61]. The atmosphere during the cooling process was only Ar-5%H_2 to prevent steam condensation on the samples and CsOH, which might differ the real weight changes on them during the heating process. After the gas-solid interaction test had been completed, both samples and CsOH were weighted inside the inert gas glovebox and proceeded to a dissolution process before the characterization.

4.4 Results and discussion

Table 4.1 and Fig. 4.3 present the information of weight changes on samples and the image of samples after the gas-solid interaction test, respectively. It was found that the NKL calsils and JIC calsils obtained approximately the same weight gain ratio of about 67% while the calsil obtained about 48%. There are some underlying factors to induce this weight gain, for instance the density or specific surface area. However, the current data that could be compared among these calcils is the density which definitely shows at the same nominal

volume (25 mm^3), the weight of NKL calsil and JIC calsil are two to three times lower than calsil. This implies that those lower-density calsils enable more CsOH penetration to the sample matrix. If we hold this presumption, then the final amount of cesium compound on these lower density calsils should be higher.

Table 4.1 Weight changes on samples.

Material	Weight before the test (g)	Weight after the test (g)	Weight gain (g)	Weight gain ratio (%)
Calsil	0.147	0.217	0.0700	47.8
JIC calsil-1	0.0592	0.0996	0.0404	68.2
JIC calsil-2	0.0555	0.0928	0.0373	67.2
NKL calsil-1	0.0646	0.108	0.0431	66.7
NKL calsil-2	0.0532	0.0888	0.0356	66.9
Total			0.226	

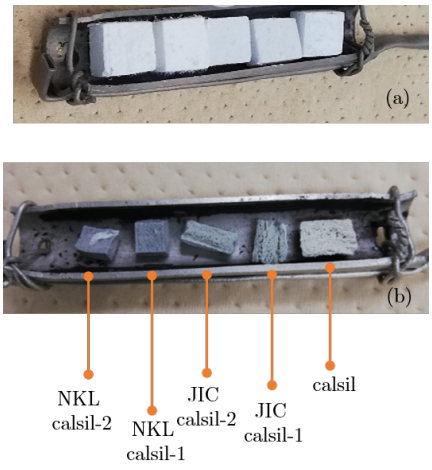

Fig. 4.3 Condition of samples (a) before and (b) after the gas-solid interaction test.

The concentration of cesium gaseous phase in the furnace was calculated based on the evaporated amount of CsOH which then divided by the obtained volume through ideal gas law. This principle is more reliable in the actual system rather than an estimation from equilibrium vapor source of CsOH at the source temperature as demonstrated by Bowsher et al [62], due to the assumption of equilibrium does not always prevail [53]. Table 4.2 provides the estimated cesium hydroxide concentration in this study. If we assume that no condensation or reaction occurred on Ni inner tube, then 48% of this evaporated CsOH (i.e., weight loss) is chemisorbed on all calsils.

Table 4.2 Weight changes and the estimated concentration of cesium hydroxide.

Material	Weight before test (g)	Weight after test (g)	Weight loss (g)	Concentration (μg/cm³)
CsOH	4.53	4.06	0.470	7.37

The morphological changes in the samples were examined and presented in Fig. 4.4. The fibers which existed on all calsils were decomposed after the test. It was found that similar morphology of particle agglomerates was formed on these calsils. Hence the elements distribution analysis using EDS elemental mapping and crystal phase identification using X-ray diffraction would be required.

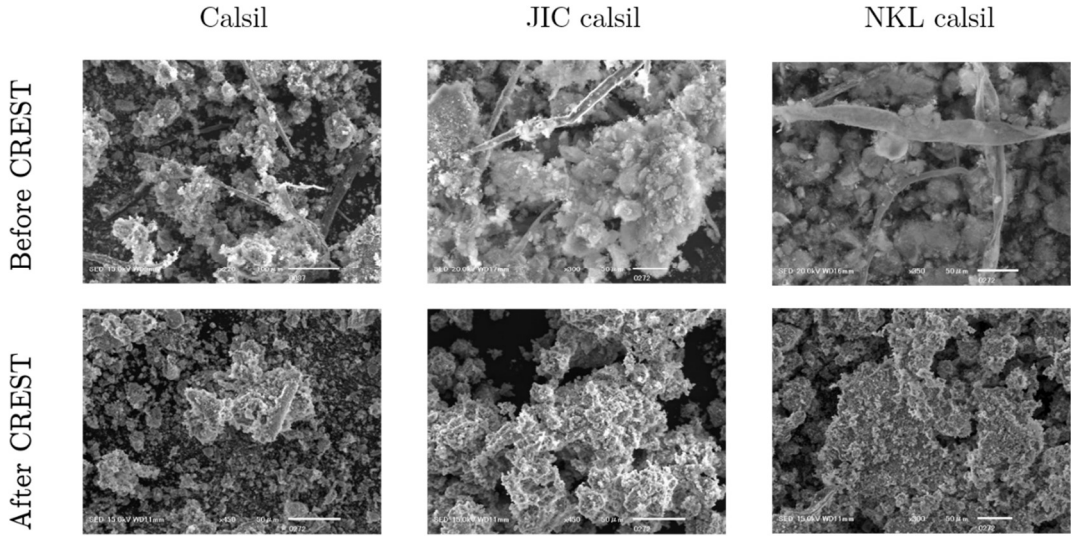

Fig. 4.4 Secondary electron images of calsil, JIC calsil and NKL calsil before and after the gas-solid interaction test.

The XRD patterns comparison, as shown in Fig. 4.5, are for all samples of calsil after the dissolution process, along with the XRD pattern of TG-DTA sample S12 (i.e., calsil mixed with CsOH; temperature up to 1100°C under Ar-4%H_2-20%H_2O), and those calsils before the gas-solid interaction test. In the previous chapter, it had been found that after the heat treatment, $CsAlSiO_4$, $CaSiO_3$ and Ca_2SiO_4 crystal phases were identified where $CaSiO_3$ was obtained due to xonotlite crystal transformation to wollastonite ($Ca_6Si_6O_{17}(OH)_2$ → $CaSiO_3$), while $CsAlSiO_4$ and Ca_2SiO_4 were obtained due to the reaction with CsOH (i.e., Eqs. 3.3 and 3.6 of Chapter 3). In the present gas-solid interaction study where CsOH being transported by steam flow toward calsil location and

analyzed whether the similar interaction occurred as when they were initially in contact (TG-DTA sample), it was revealed and affirmed with the XRD pattern that cesium aluminum silicate was **formed** by the interaction of cesium hydroxide with calsil.

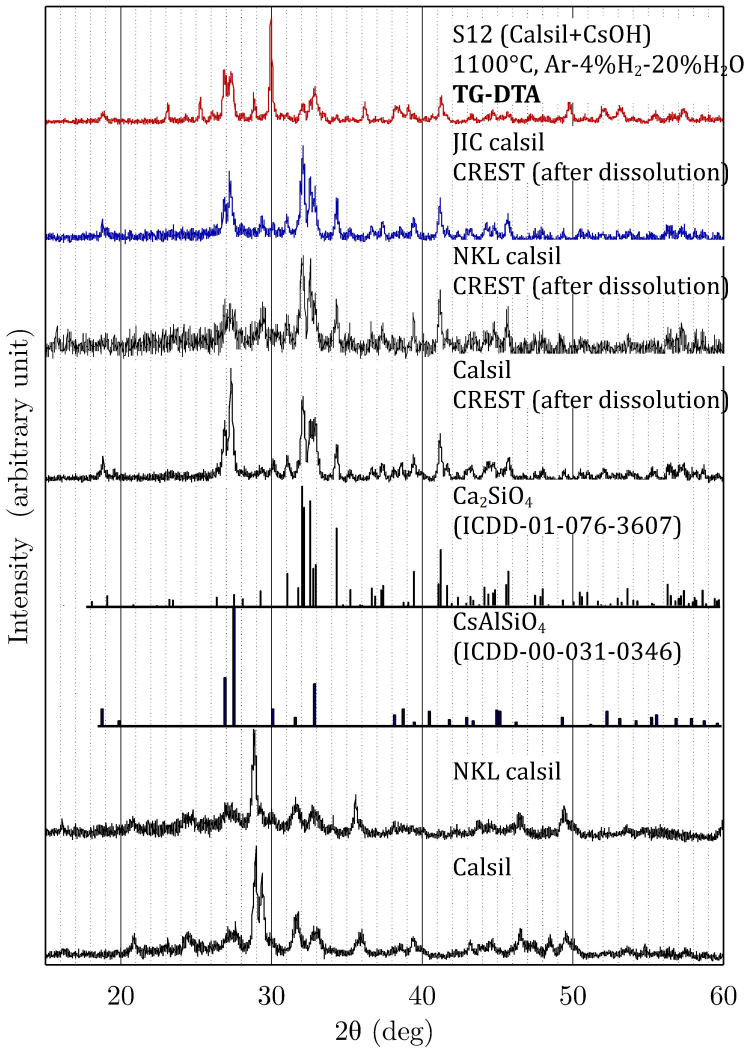

Fig. 4.5 Comparison of XRD patterns of calsil, NKL calsil, JIC calsil before and after the heating test as well as sample S12.

The quantitative analyses of those calsil samples by using the RIR method in the Rigaku integrated X-ray powder diffraction software, PDXL© version 2.7.2.0, are given in Table 4.3 along with their respective apparent density. In average, the amount of Ca_2SiO_4 formed in calsils after the interaction is about 89.7 wt%, followed by $CsAlSiO_4$ with 10.3 wt%. No significant difference of cesium aluminum silicate among these samples implying that most of the weight gain (Table 4.1) obtained after the interaction was a result of the coexistence of water-soluble Cs compound inside the calcium silicate.

Table 4.3 Quantitative analyses for all calsils after the gas-solid interaction test.

Material	Apparent density (g/cm^3)	Al amount in sample before heating test (wt%)	Ca_2SiO_4 (wt%)	$CsAlSiO_4$ (wt%)
Calsil	0.44[1]	0.94	91	9.0
JIC calsil	0.13 [56]	0.78	88	12
NKL calsil	0.12 [55]	0.78	90.0	10.0

The elemental mapping for calsil and JIC calsil is given in Fig. 4.6 for the comparison. The elemental mapping of NKL calsil is not presented in the main text to avoid redundant information, instead, it is supplemented in Appendix B.4.

[1] Calculated based on the initial weight before the gas-solid interaction test

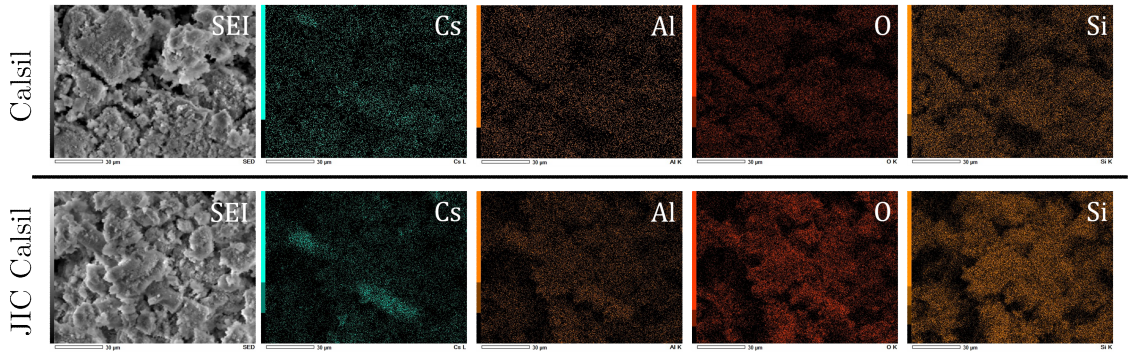

Fig. 4.6 EDS elements mapping of calsil and JIC calsil after the dissolution.

As shown in Fig. 4.6, the Cs, Al, O, and Si are congruently distributed for both calsils. Cesium compound is more concentrated on the remaining fiber. This is because at this location—before the gas-solid interaction test—Al is in higher weight percentage comparing to the particles agglomerate thus resulting in more cesium aluminum silicate to be formed.

The infrared spectra of those calsils after the gas-solid interaction test are shown in Fig 4.7 along with the reference spectra for Ca_2SiO_4 and $CsAlSiO_4$, to show the vibrational modes in respective bands. All these calsils are identical to the assigned vibrations except for band at 449 cm^{-1} in NKL calsil which attributed to the bending mode of Al–O (denoted by δ) and/or Si–O [63].

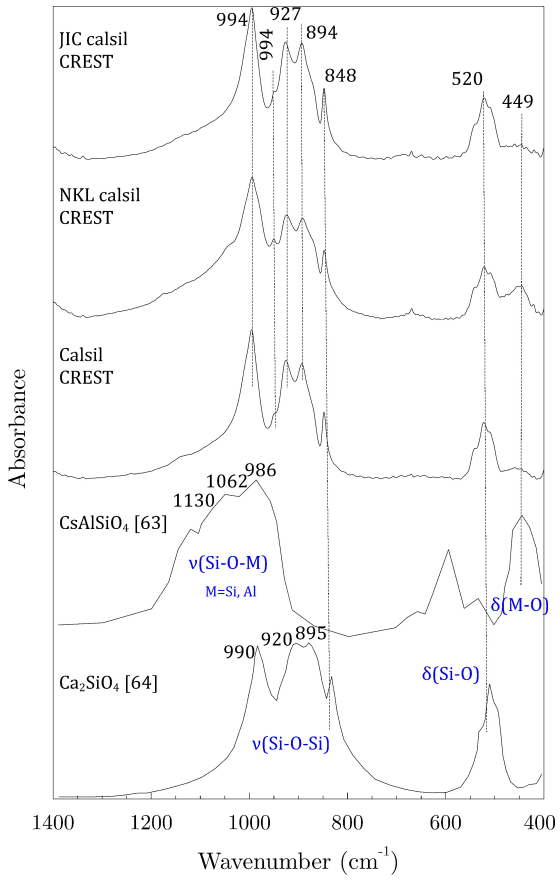

Fig. 4.7 IR spectra of calsil, NKL calsil, and JIC calsil after gas-solid interaction test, and the spectra of Ca_2SiO_4 and $CsAlSiO_4$.

The strongest band at 994 cm^{-1} is likely due to stretching vibrations of Si–O–Al (denoted by ν) from CsAlSiO4 and Si–O–Si from Ca_2SiO_4. The vibrational bands of 994, 927, 895, and 848 cm^{-1} are stretching vibrations of Si–O–Si from Ca_2SiO_4 and band at 520 cm^{-1} is bending vibrational mode of Si–O from Ca_2SiO_4 [64].

4.5. Chapter summary

The gas-solid interaction test between calcium silicate insulator materials (calsil) and cesium hydroxide (CsOH) was experimentally investigated under Ar-4%H_2-20%H_2O atmosphere with a temperature of 800°C. The temperature was chosen based on the suggested reaction temperature in the thermochemical investigation. The interaction was realized by using a horizontal electric furnace where cesium hydroxide was vaporized in the upstream of furnace and then transported by steam flow to the downstream where calcium silicates were located. After the gas-solid interaction test, series of characterizations were conducted including crystallography, elemental, morphological, and vibrational analyses. The XRD patterns of those calsils had been changed from their original crystal phase of xonotlite ($Ca_6Si_6O_{17}(OH)_2$) to $CsAlSiO_4$ and Ca_4SiO_4 meaning that the interaction with gaseous cesium hydroxide prevailed. Additionally, to support the result of cesium aluminum silicate formation, the elemental distribution analyses of Cs, Si, O, and Al were performed using the EDS which showed the congruent distribution in the samples after this gas-solid interaction test. Infrared spectra of those samples also showed a similar stretching vibrational mode of Si-O-Si(Al) at 994 cm^{-1} and bending vibration mode of (Al)Si-O at 449 cm^{-1} to that of $CsAlSiO_4$ reference. These gas-solid interaction test results have confirmed the

previously predicted cesium compound in TG-DTA analyses, $CsAlSiO_4$, would be retained in the calcium silicate after the interaction with cesium hydroxide as an end-product.

Chapter 5 Conclusions and future work

5.1 Conclusions

The interaction of cesium with calcium silicate insulator materials had been experimentally investigated to reveal its fundamental information and possible post-interaction retention of cesium under different temperature conditions. The quick combined analyses throughout the thesis showed that cesium was chemisorbed on calcium silicate and in particular at the higher temperature it was retained in the end-product as cesium aluminum silicate. Considering the similar elements that might exist in other structural materials inside the primary containment vessels (PCV), the findings here had opened new insight of cesium chemistry with those alike materials under nuclear severe accident conditions. At room-temperature condition, the calcium silicate insulator material—in the scope of the present study—effectively adsorbed cesium from the solution about 44% in few hours. The analyses had shown this interaction was chemisorption. Despite of this uptake percentage, it clearly unveiled the ability of this material to retain cesium. The plausible consequences of this are giving the fate of late-phase cesium release upon external forces to which could induce further implications. Hence, understanding the higher temperature atmospheric

effect on the interaction would be imperative to probe the stability of the retained cesium.

The dedicated investigation on thermochemical analyses by using thermogravimetry-differential thermal analysis (TG-DTA) was conducted to unveil whether or not the interaction prevailed at the higher temperature and stably formed in the material. For this specific purpose, the selected simulant fission product was cesium hydroxide (CsOH). The interaction was experimentally investigated under reducing and oxidizing atmosphere with temperature up to 1100°C. It was found that two types of pre-conditioned calcium silicate insulation materials led to distinct reaction temperature with CsOH: 575°C to 730°C for calsil while 700°C to 1100°C for PHT calsil. Despite of the reaction temperatures and difference in their initial chemical compounds (calsil: $Ca_6Si_6O_{17}(OH)_2$; PHT calsil: $CaSiO_3$), the end product of those calsils after subjected to a reaction with CsOH in temperature up to 1100°C yielded similar XRD pattern regardless the atmosphere condition, which corresponded to the formation of cesium aluminum silicate: $CsAlSiO_4$. The benchmark heating tests using reagent-grade $CaSiO_3$ were supplemented to the analyses to prove the previous findings of such a $CsAlSiO_4$ formation in calsil and PHT calsil. The results have proved that such a cesium aluminum silicate was not formed in all

benchmark samples but in turn yielding the Cs water-soluble compound and Ca_2SiO_4. Therefore, based upon this information (i.e., the temperature of reaction prevailed; products after the interaction) the real case gas-solid interaction was realized.

In the effort of emulating real interaction between calcium silicate insulator material and cesium hydroxide, the gas-solid interaction test was investigated under Ar-4%H_2-20%H_2O atmosphere with the temperature of 800°C. The temperature was chosen based on the suggested reaction temperature in the thermochemical investigation. The interaction was realized by using a horizontal electric furnace where cesium hydroxide was vaporized in the upstream of the furnace and then transported by steam flow to the downstream where calcium silicates were located. To elaborate on the prevalence of interaction, two additional calcium silicates from different manufacturers were included in the test. After the gas-solid interaction test, series of characterizations were conducted including crystallography, elemental, morphological, and vibrational analyses. The combined analyses on those calsils had proved that the end-products contained $CsAlSiO_4$ and Ca_2SiO_4, and had affirmed the interactions with cesium hydroxide gaseous phase. At this point, the presence of aluminum in the calcium silicate insulator material arose as the key factor in the high-temperature

interaction. Without such an element, cesium could not be stably retained in the calcium silicate insulator material. Figure 5.1 collectively combines the investigation at high-temperature atmospheric conditions. The crystal structures used in the illustration were rendered by Jmol [65].

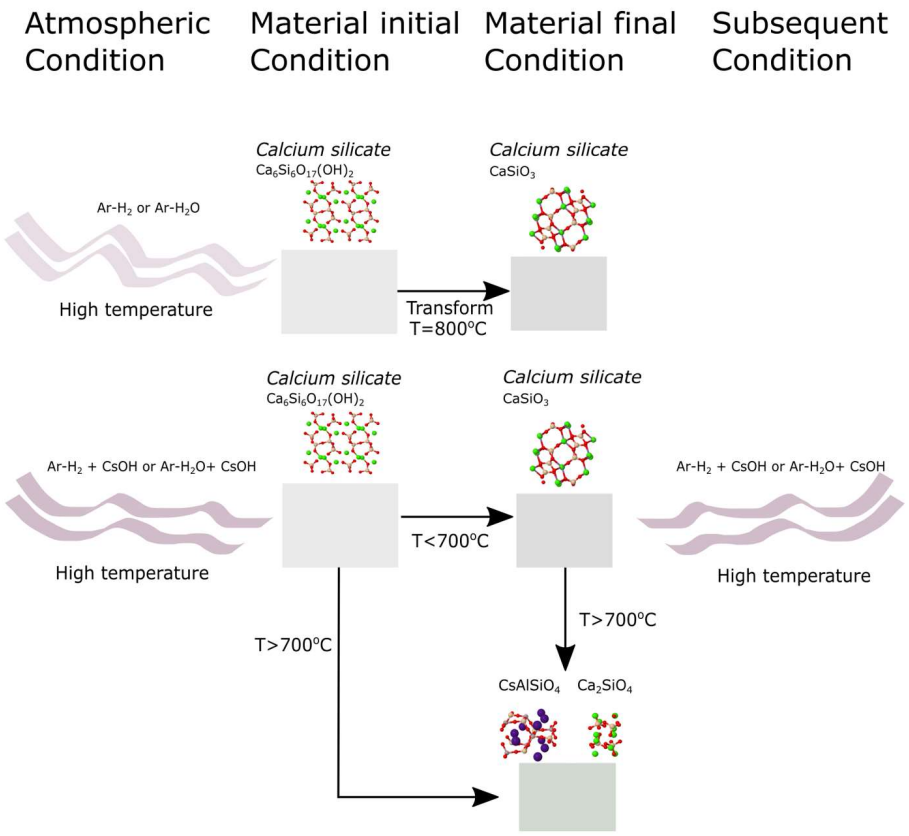

Fig. 5.1 Effect of various high-temperature atmospheric conditions on calcium silicate insulator material.

5.2 Future work

It had been noticed in the main chapter that a parametric study on the threshold of the aluminum amount in calcium silicate would be an underlying

case. However, considering the high cost for the purification technique of aluminum, it was not possible to be realized in the present study. This path will open new insight on the calcium silicate insulation manufacturing process since most of the starting materials at a certain limit contain alumina. The reduction of alumina would induce greater consequences on finding the alternative starting materials that still could maintain the physical properties of the insulation and withstand the harsh environment.

The inclusion of other structural materials such as concrete and stainless steel during the gas-solid interaction test would be imperative in the next step. The transport itself will involve a sequential process from the reactor core where these structural materials are chosen as a representation of material at each stage when FPs transportation progress into the lower temperature region. To which stainless steel represents the internal structure of the reactor and coolant system; piping insulation (i.e. calcium silicate) represents material existed just after the coolant system; concrete represents the primary containment vessel and reactor building material. Therefore, the integrated test involving the materials would provide a better understanding of the fission product interaction.

Bibliography

[1] Tokyo Electric Power Company. Report on the investigation and study of unconfirmed/unclear matters in the Fukushima nuclear accident. Japan: Tokyo Electric Power Company (TEPCO); 2014, Summary report - progress report no. 2.

[2] Tokyo Electric Power Company. Evaluation of the situation of cores and containment vessels of Fukushima Daiichi nuclear power station units-1 to 3 and examination into unsolved issues in the accident progression. Japan: Tokyo Electric Power Company (TEPCO); 2017, Progress report no. 5.

[3] Sehgal, BR., & Bechta, S. Severe accident progression in the BWR lower plenum and the modes of vessel failure. *Ann. Nucl. Energy.* **93**, 28–34 (2016).

[4] Vu, B., Wang, T. S., Shih, M. H. & Soni, B. Navier-Stokes flow field analysis of compressible flow in a high pressure safety relief valve. *Appl. Math. Comput.* **65**, 345–353 (1994).

[5] Martin, P. G., Satou, Y., Griffiths, I., Richards, D. & Scott, T. Analysis of external surface irregularities on Fukushima-derived fallout particles. *Front. Energy Res.* **5**, 25 (2017).

[6] Martin, P. G., Louvel, M., Cipiccia, S., Jones, C. P., Batey, D. J., Hallam, K. R., Yang, I. A. X., Satou, Y., Rau, C., Mosselmans, J. F. W., Richards, D. A. & Scott, T. B. Provenance of uranium particulate contained within Fukushima Daiichi nuclear power plant unit 1 ejecta material. *Nat Commun.* **10**, 2801 (2019).

[7] Satou, Y. [Radioactive particles emitted at 1FNPS accident – Overview of insoluble cesium particle]. Nihon-Genshiryoku-Gakkai Shi (*J. At. Energy Soc. Jpn.*). **61**(6), 446-448 (2019) [in Japanese].

[8] Allen, G. C., Bowsher, B. R, Dickinson, S., Fotios, G. M., Nichols, A. L. & Wild, R. K. Surface studies of the interaction of cesium hydroxide vapor with 304 stainless steel. *Oxid. Met.* **28**, 33–59 (1987).

[9] Haste, T., Payot, F. & Bottomley, P. D. W. Transport and deposition in the Phébus FP circuit. *Ann. Nucl. Energy*. **61**, 102–121 (2013).

[10] Kalilainen, J., Kärkelä, T., Zilliacus, R., Tapper, U., Auvinen, A. & Jokiniemi, J. Chemical reactions of fission product deposits and iodine transport in primary circuit conditions. *Nucl. Eng. Des*. **267**, 140–147 (2014).

[11] Di Lemma, F. G., Nakajima, K., Yamashita, S. & Osaka, M. Experimental investigation of the influence of Mo contained in stainless steel on Cs chemisorption behavior. *J. Nucl. Mater*. **484**, 174–182 (2017).

[12] Kobata, M., Okane, T., Nakajima, K., Suzuki, E., Ohwada, K., Kobayashi, K., Yamagami, H. & Osaka, M. Chemical form analysis of reaction products in Cs-adsorption on stainless steel by means of HAXPES and SEM/EDX. *J. Nucl. Mater.* **498**, 387–394 (2018).

[13] Chang, S. J., Furuya, H., Fujii, T. & Idemitsu, K. Corrosion of austenitic stainless steel in steam containing cesium hydroxide, *J. Nucl. Sci. Technol.* **29**(8), 753-761 (1992).

[14] Akers, D. W. & Roybal, G. S. Examination of concrete samples from the TMI-2 reactor building basement. United States: EG and G Idaho, Inc; 1987, Report no. GEND-INF-081.

[15] Maeda, K., Sasaki, S., Kumai, M., Sato, I., Suto, M., Ohsaka, M., Goto, T., Sakai, H., Chigira, T. & Murata, H. Distribution of radioactive nuclides of boring core samples extracted from concrete structures of reactor buildings in the Fukushima Daiichi Nuclear Power Plant. *J. Nucl. Sci. Technol.* **51**(7–8), 1006–1023 (2014).

[16] Do, T. M. D., Sujatanond, S. & Ogawa, T. Behavior of cesium molybdate, Cs_2MoO_4, in severe accident conditions. (1) Partitioning of Cs and Mo among gaseous species. *J. Nucl. Sci. Technol.* **55**, 348–355 (2018).

[17] Nuclear and Industrial Safety Agency. Report on emergency core cooling system strainer and containment vessel recirculation sump screen blocking event and status of measures on boiling water nuclear power plant. Japan: Nuclear and Industrial Safety Agency (NISA); 2006, 44th Nuclear Safety Commission, Report material no. 2 [in Japanese].

[18] Tokyo Electric Power Company. Unit 2 Primary Containment Vessel Investigation at Fukushima Daiichi Nuclear Power Station (Investigation results by the self-propelled investigation device). Japan: Tokyo Electric Power Company (TEPCO); 2017. Accessed on June 6, 2017 from https://www7.tepco.co.jp/wp-content/uploads/hd03-02-03-004-001-handouts_170216_01-e.pdf.

[19] Schlegel, M. L., Pointeau, I., Coreau, N. & Reiller, P. Mechanism of europium retention by calcium silicate hydrates: an EXAFS study. *Environ. Sci. Technol.* **38**(16), 4423–4431 (2004).

[20] Tits, J., Wieland, E., Muller, C. J., Landesman, C. & Bradbury, M. H. Strontium binding by calcium silicate hydrates. *J. Colloid Interf. Sci.* **300**(1), 78–87 (2006).

[21] Gaona, X., Dahn, R., Tits, J., Scheinost, A. C. & Wieland, E. Uptake of Np(IV) by C-S-H phases and cement paste: an EXAFS study. *Environ. Sci. Technol.* **45**(20), 8765–8771 (2011).

[22] Tits, J., Fujita, T., Harfouche, M., Dahn, R., Tsukamoto, M. & Wieland, E. Radionuclide uptake by calcium silicate hydrates: Case studies with Th(IV) and U(VI). Switzerland: Paul Scherrer Institut (2014).

[23] Steve, L. P., Kowalski, M., Pšenička, M., Klinkenberg, M., Rohmen, S., Bosbach, D. & G. Deissmann. Uptake of ^{226}Ra in cementitious systems: a complementary solution chemistry and atomistic simulation study, *Appl. Geochem.* **96**, 204–216 (2018).

[24] Hassan, H. S., Kenawy, S. H., El-Bassyouni, G. T., Hamzawy, E. M. A. & Hassan, R. S. Sorption behavior of cesium and europium radionuclides onto nano-sized calcium silicate. *Particul. Sci. Technol.* (2018).

[25] Zheng, Q. & Wang, W. Calcium silicate based high efficiency thermal insulation. *Br. Ceram. Trans.* **99**(4), 187–190 (2000).

[26] Leite, F. H. G., Almeida, T. F., Faria, R. T. & Holanda, J. N. F. Synthesis and characterization of calcium silicate insulating material using avian eggshell waste. *Ceram. Int.* **43**, 4674–4679 (2017).

[27] El-Hemaly, S. A. S., Mitsuda, T. & Taylor, H. F. W. Synthesis of normal and anomalous tobermorites. *Cem. Concr. Res.* **7**(4), 429–438 (1977).

[28] Shaw, S., Clark, S. M. & Henderson, C. M. B. Hydrothermal formation of the calcium silicate hydrates, tobermorite ($Ca_5Si_6O_{16}(OH)_2 \cdot 4H_2O$) and xonotlite ($Ca_6Si_6O_{17}(OH)_2$): An in situ synchrotron study. *Chem. Geol.* **167**, 129–140 (2000).

[29] Meller, N., Hall, C. & Phipps, J. S. A new phase diagram for the CaO–Al_2O_3–SiO_2–H_2O hydroceramic system at 200°C. *Mater. Res. Bull.* **40**, 715–723 (2005).

[30] Kim, S. H., Rethinasabapathy, M., Haldorai, Y., Lee, G. W., Choe, S. R., Kang, S. C., Han, Y. K., Roh, C., Cho, W. S. & Huh, Y. S. Porous 3D Prussian blue/cellulose aerogel as a decorporation agent for removal of ingested cesium from the gastrointestinal tract. *Sci. Rep.* **8**, 1–14 (2018).

[31] Long, H., Wu, P. & Zhu, N. Evaluation of Cs^+ removal from aqueous solution by adsorption on ethylamine-modified montmorillonite. *Chem. Eng. J.* **225**, 237–244 (2013).

[32] Xia, M. *et al.* The adsorption of Cs^+ from wastewater using lithium-modified montmorillonite caged in calcium alginate beads. *Chemosphere*. **203**, 271–280 (2018).

[33] Ebadi, A., Mohammadzadeh, J. S. S. & Khudiev, A. What is the correct form of BET isotherm for modeling liquid phase adsorption? *Adsorption*. **15**, 65–73 (2009).

[34] Brunauer, S., Emmet, P.H. & Teller, E. Adsorption of gases in multi-molecular layers. *J. Am. Chem. Soc.* **60**, 309–319 (1938).

[35] Farley, K. J., Dzombak, D. A. & Morel, F. M. M. A surface precipitation model for the sorption of cations on metal oxides. *J. Colloid Interface Sci.* **106**, 226–242 (1985).

[36] Lützenkirchen, J. & Behra, P. On the surface precipitation model for cation sorption at the (hydr)oxide water interface. *Aquat. Geochemistry*. **1**, 375–397 (1995).

[37] Zheng, X., Dou, J., Yuan, J., Qin, W., Hong, X. & Ding, A. Removal of Cs^+ from water and soil by ammonium-pillared montmorillonite/Fe_3O_4 composite, *J. Environ. Sci.* **56**, 12–24 (2017).

[38] Alamudy, H. A. & Cho, K. Selective adsorption of cesium from an aqueous solution by a montmorillonite-prussian blue hybrid. *Chem. Eng. J.* **349**, 595–602 (2018).

[39] Mostafa, N. Y., Shaltout, A. A., Omar, H. & Abo-El-Enein, S. A. Hydrothermal synthesis and characterization of aluminium and sulfate substituted 1.1 nm tobermorites. *J. Alloys Compd.* **467**, 332–337 (2009).

[40] Yu, P., Kirkpatrick, R. J., McMillan, P. F., Poe, B. & Cong, X. Structure of Calcium Silicate Hydrate (C-S-H): Near-, Mid-, and Far-Infrared Spectroscopy. *J. Am. Ceram. Soc.* **82**, 742–748 (2010).

[41] Hartmann, A., Schulenberg, D. & Buhl, J.-C. Investigation of the Transition Reaction of Tobermorite to Xonotlite under Influence of Additives. *Adv. Chem. Eng. Sci.* **5**, 197–214 (2015).

[42] Miwa, S., Ducros, G., Hanus, E., Bottomley, P. D. W., Van Winckel, S. & Osaka, M. Release and transport behaviors of non-gamma-emitting fission products and actinides in steam and hydrogen atmospheres. *Nucl. Eng. Des.* **326**, 143–149 (2018).

[43] West, A. R. Solid State Chemistry and its application– Second edition, student edition. John Wiley & Sons Ltd. London, 314–320 (2014).

[44] Dent, L. S. & Taylor, H. F. W. The dehydration of xonotlite. *Acta. Cryst.* **9**, 1002–1004 (1956).

[45] Meyer, J. W. & Jaunarajs, K. L. Synthesis and crystal chemistry of gyrolite and reyerite. *Am. Mineral.* **46**, 913–933 (1961).

[46] Shaw, S., Henderson, C. M. B. & Komanschek, B. U. Dehydration/recrystallization mechanisms, energetics, and kinetics of hydrated calcium silicate minerals: an in situ TGA/DSC and synchrotron radiation SAXS/WAXS study. *Chem. Geol.* **167**, 41–159 (2000).

[47] Liljenzin, J. O. & Schock, W. Fission product transport, in Krischer, W.(ed). & Rubinstein, M. C.(ed). The Phebus fission product project: Presentation of the experimental programme and test facility. Session II, State of the art deduced from previous large experiments. Elsevier Applied Science. London, 64-84 (1992).

[48] Barin, I. Thermochemical data of pure substances. VCH Verlagsgesellschaft mbH. Weinheim (Germany), (1995).

[49] Taylor, P, DeVaal S, D. & Owen, D. G. Stability relationships between solid cesium aluminosilicates in aqueous solutions at 200°C. *Can. J. Chem.* **67**, 76-81 (1989).

[50] Ball, R. G. J., Bowsher, B. R., Cordfunke, E. H. P., Dickinson, S. & Konings, R. J. M. Thermochemistry of selected fission product compounds. *J. Nucl. Mater.* **201**, 81-91 (1993).

[51] Spencer, P. J. The thermodynamic properties of silicates. National Physical Laboratory (NPL). NPL Report Chemistry. **21**, (1973).

[52] Lide, D. R. CRC Handbook of Chemistry and Physics 88th Edition. CRC Press, Taylor & Francis, Boca Raton, 4-57 (2007).

[53] Nishioka, S., Nakajima, K., Suzuki, E. & Osaka, M. An experimental investigation of influencing chemical factors on Cs-chemisorption behavior onto stainless steel. *J. Nucl. Sci. Technol.* **56**, 988–995 (2019).

[54] Ong, S. P., Richards, W. D., Jain, A., Hautier, G., Kocher, M., Cholia, S., Gunter, D., Chevrier, V. L., Persson, K. & Ceder, G. Python Materials

Genomics (pymatgen): A Robust, Open-Source Python Library for Materials Analysis. *Comput. Mat. Sci.* **68**, 314–319 (2013).

[55] Nippon Keical, Ltd. Keical ace super silica. http://nippon-keical.co.jp/en/products.html. Accessed 25 October 2018 (2018).

[56] Japan Insulation Co., Ltd. Daipalite. https://www.jic-bestork.co.jp/modules/smartsection/item.php?itemid=271. Accessed 25 October 2018 (2018).

[57] Meisei Industrial Co., Ltd. Keical ace. http://www.meisei-kogyo.co.jp/en/seihin/keicalace/index.html. Accessed 25 November 2019 (2019).

[58] A&A Material Corporation. Super feather silica cover. https://www.aa-material.co.jp/eng/products/ip/ti/silica/hr/super_feather_silica.html. Accessed 25 November 2019 (2019).

[59] Nichias Corporation. Keical ace super silica (ケイカルエース・スーパーシリカ). https://www.nichias.co.jp/products/download/PDF/I37.PDF. Accessed 25 November 2019 (2019).

[60] Nakajima, K., Suzuki, E., Miyahara, N. & Osaka, M. An experimental investigation for atmospheric effects on Cs chemisorption onto stainless steel. *Prog. Nucl. Sci. Technol.* **5**, 168–170 (2018).

[61] Di Lemma, F. G., Nakajima, K., Yamashita, S. & Osaka, M. Surface analyses of cesium hydroxide chemisorbed onto type 304 stainless steel. *Nucl. Eng. Des.* **305**, 411–420 (2016).

[62] Bowsher, B. R., Dickinson, S. & Nichols, A. L. High temperature studies of simulant fission products: part III, Temperature-dependent interaction of

cesium hydroxide vapor with 304 stainless steel. Winfrith Newburgh (Dorset): AEE Winfrith, Technology Division; AEEW-R 1863 (1990).

[63] Ali Ghrear, T. M., Cheong, Y. W., Lim, G. K., Chateigner, D., Ling, T. C., Tan, S. H. & Ng, E. P. Fast, low-pressure, low-temperature microwave synthesis of ABW cesium aluminosilicate zeolite nanocatalyst in organotemplate-free hydrogel system. *Mater. Res. Bull.* (2019). *In press*.

[64] Handke, M. & Ptak, W. Ir and Raman studies of the stabilization of β-Ca_2SiO_4. *Ceramurg. Int.* **4**, 75–78 (1978).

[65] Jmol: an open-source Java viewer for chemical structure in 3D. http://www.jmol.org/.

Acknowledgment

All praise to Allah and may peace be upon His messenger. I would like to deliver my depth gratitude to the following people and foundations which supported me through this doctoral program:

- Prof. Koji Okamoto, the academic supervisor, who again was willing to supervise me after the Master's degree, for the kindness, the great supervision, and the constructive comments. I deeply appreciate when introducing me to Assoc. Prof. Takumi Saito which had made me progressed very well in analytical chemistry.
- Assoc. Prof. Takumi Saito, the academic co-supervisor, for great supervision, supports and helps. In particular, to spare time in his tight schedule to come to the JAEA Tokai office for the regular meeting. It was my honor to learn a lot of analytical chemistry from him.
- Dr. Masahiko Osaka and Dr. Kunihisa Nakajima of JAEA for the kindness to accept me as the special researcher student in the Group (Development Group for LWR Advanced Technology, NSEC), which in fact the opportunity had made me able to complete the main parts

of my doctoral thesis. Also my gratitude to the member of the Group for all the help during the TG-DTA, CREST, XRD, and SEM/EDS.

- Assoc. Prof. Nejdet Erkan for the constructive discussion at the beginning of this doctoral study.
- Mrs. Hisako Komatsu and Mrs. Junko Inoue who have been truly kind and helpful dealing with the administrative matters during my study, especially Mrs. Hisako Komatsu who dealt the administrative procedure of doctoral course during my six-month leave to Indonesia.
- My mother, Nurdjana Badjeber, who in every aspect being my figure to pursue the higher academic, and for the invaluable love and supports.
- My beloved wife, Asti Yuniar Sasmaya for the patience and kindness to support me in every situation.
- The SEUT-RA and Tokio Marine Kagami Memorial Foundation for the financial supports during the doctoral program are acknowledged.

Appendix A Experiment configurations

A.1 Batch-type adsorption experiment configuration

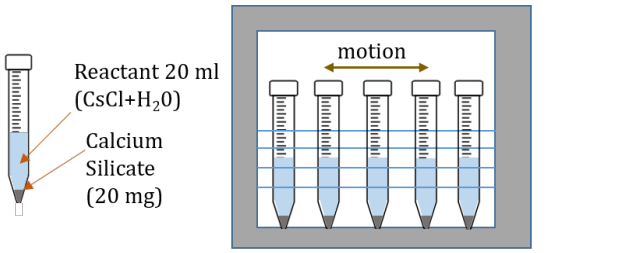

Fig. A.1 Schematic illustration of batch-type adsorption experiment at the room-temperature condition

A.2 Thermochemical investigation experiment configuration

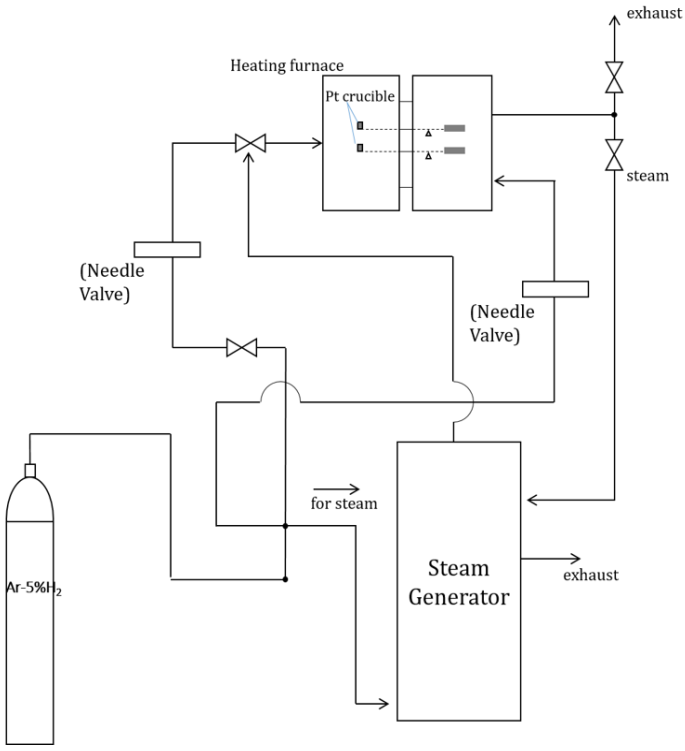

Fig. A.1 Schematic illustration of TG-DTA heating furnace with the integrated steam generator.

Appendix B Additional results

B.1 Particle size analysis of calcium silicate

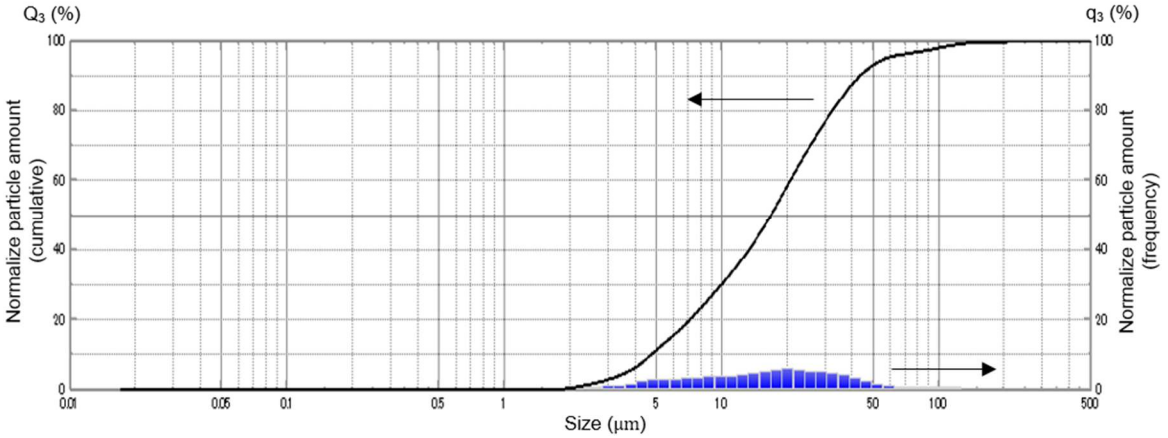

Fig. B.1 Results of particle size analysis of calcium silicate using laser diffraction size analyzer

B.2 X-ray fluorescence results

Table B.1 Summarized result of XRF for calcium silicate

Element	%wt	Method	Analysis line
O	43.2	Quantitative-FP	O Ka
Ca	30.6	Quantitative-FP	Ca Ka
Si	18.4	Quantitative-FP	Si Ka
C	5.13	Quantitative-FP	C Ka
Al	0.944	Quantitative-FP	Al Ka
Fe	0.696	Quantitative-FP	Fe Ka
Mg	0.363	Quantitative-FP	Mg Ka
S	0.174	Quantitative-FP	S Ka
K	0.156	Quantitative-FP	K Ka

B.3 Quantitative analysis of sample S5

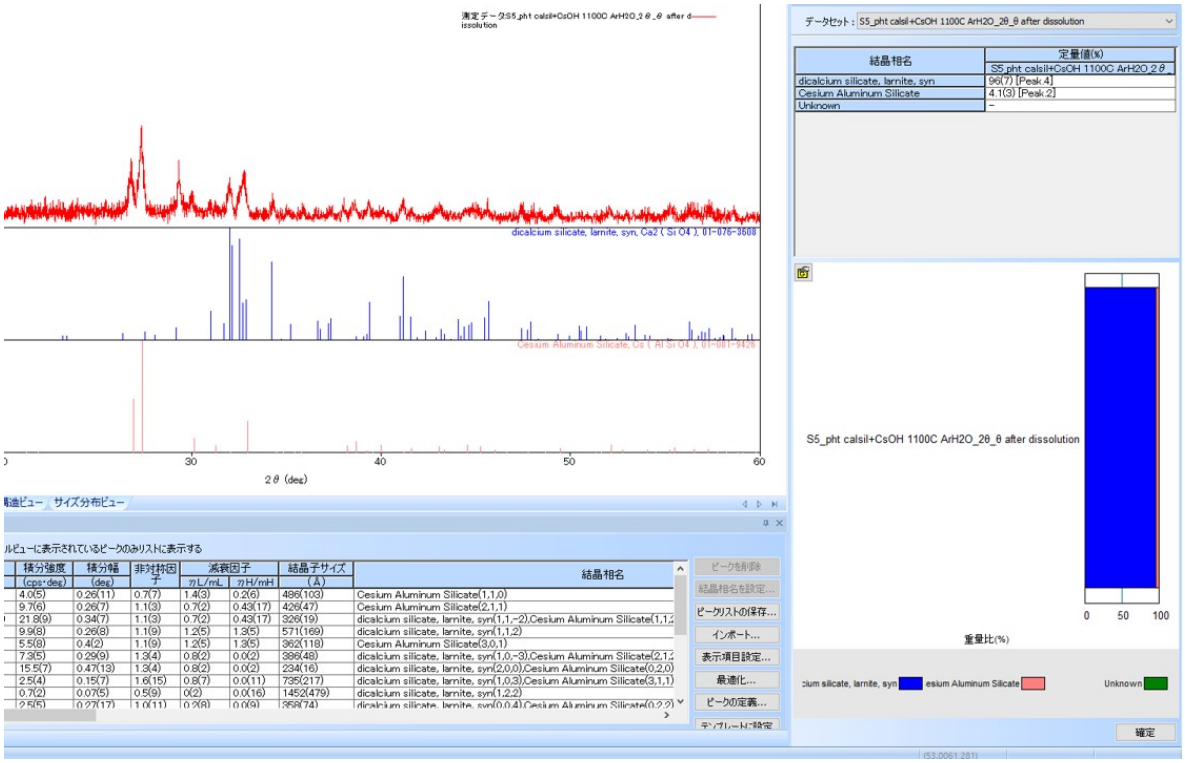

Fig. B.2 Graphic user interface of PDXL© showing quantification process of sample S5 (PHT calsil mixed with CsOH)

B.4 EDS element mapping of NKL calsil after the experiment

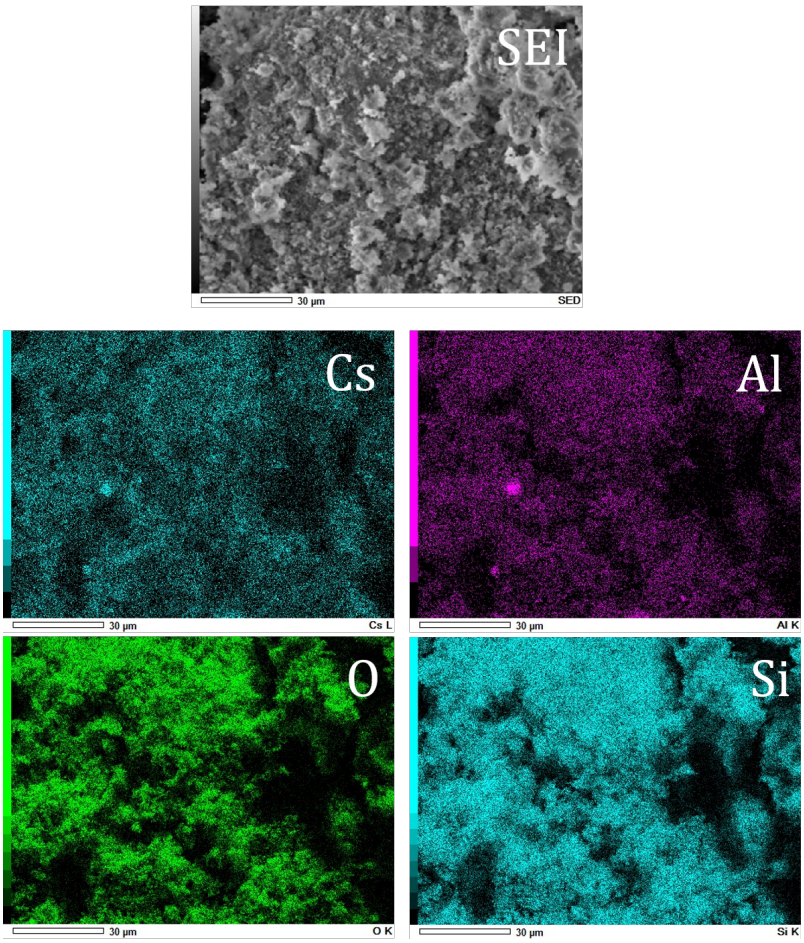

Fig. B.3 Element mapping of NKL calsil after the gas-solid interaction test with cesium hydroxide.